



Calhoun: The NPS Institutional Archive
DSpace Repository

Faculty and Researchers

Faculty and Researchers Collection

2006

Vortex evolution due to straining

Graves, L. P.; J. C. McWilliams; Montgomery, M. T.

Vortex evolution due to straining: A mechanism for dominance of strong, interior anticyclones, *Geophys. & Astrophys. Fluid Dynamics*, 100, 151-183: 2006, Graves, L. P., J. C. McWilliams, and M. T. Montgomery
<http://hdl.handle.net/10945/36929>

Downloaded from NPS Archive: Calhoun



Calhoun is a project of the Dudley Knox Library at NPS, furthering the precepts and goals of open government and government transparency. All information contained herein has been approved for release by the NPS Public Affairs Officer.

Dudley Knox Library / Naval Postgraduate School
411 Dyer Road / 1 University Circle
Monterey, California USA 93943

<http://www.nps.edu/library>

Vortex evolution due to straining: a mechanism for dominance of strong, interior anticyclones

LEE PAUL GRAVES[†], JAMES C. MCWILLIAMS^{*†} and
MICHAEL T. MONTGOMERY[‡]

[†]Department of Atmospheric and Oceanic Sciences, UCLA, Los Angeles,
CA 90095-1565, USA

[‡]Department of Meteorology, Naval Postgraduate School, Monterey, CA 93943, USA;
Hurricane Research Division, NOAA/AOML, Miami, FL 33149, USA

In this article we address two questions: Why do freely evolving vortices weaken on average, even when the viscosity is very small? Why, in the fluid's interior, away from vertical boundaries and under the influence of Earth's rotation and stable density stratification, do anticyclonic vortices become dominant over cyclonic ones when the Rossby number and deformation radius are finite? The context for answering these questions is a rotating, conservative, Shallow-water model with Asymmetric and Gradient-wind Balance approximations. The controlling mechanisms are vortex weakening under straining deformation (with a weakening that is substantially greater for strong cyclones than strong anticyclones) followed by a partially compensating vortex strengthening during a relaxation phase dominated by Vortex Rossby Waves (VRWs) and their eddy–mean interaction with the vortex. The outcome is a net, strain-induced vortex weakening that is greater for cyclones than anticyclones when the deformation radius is not large compared to the vortex radius and the Rossby number is not small. Furthermore, when the exterior strain flow is sustained, the vortex changes also are sustained: for small Rossby number (i.e., the quasigeostrophic limit, QG), vortices continue to weaken at a relatively modest rate, but for larger Rossby number, cyclones weaken strongly and anticyclones actually strengthen systematically when the deformation radius is comparable to the vortex radius. The sustained vortex changes are associated with strain-induced VRWs on the periphery of the mean vortex. It therefore seems likely that, in a complex flow with many vortices, anticyclonic dominance develops over a sequence of transient mutual straining events due to the greater robustness of anticyclones (and occasionally their net strengthening).

Keywords: Vortex; Anticyclone; Vortex Rossby wave; Strain Deformation

1. Introduction

Observational and computational studies have shown that coherent vortices emerge in large-scale geophysical fluid flows under many conditions, in particular — with relevance to the present study — in the fluid's interior away from solid boundaries and under the influences of planetary rotation and stable density stratification.

*Corresponding author. Email: jcm@atmos.ucla.edu

Terrestrial examples include atmospheric vortices near the tropopause and oceanic vortices in the thermocline and abyss. Other examples can be found on the giant planets, most spectacularly the Great Red Spot of Jupiter (figure 1). Coherent vortices have also been found in computational turbulence studies of initially randomly distributed vorticity in stratified, rotating environments (McWilliams *et al.* 1994) where axisymmetrization, vertical alignment, and successive mergers of like-sign vortices cause the aggregation of vorticity into a decreasing number of larger vortices.

The emergent vortices tend to be relatively axisymmetric around a core vorticity extremum. This is true in part because an axisymmetric azimuthal circulation is a stationary solution to the conservative fluid equations in gradient-wind and hydrostatic balance, and further because linearly stable vortices are often robust to even substantial perturbations that deform them away from their axisymmetric stationary state. When perturbed, vortices tend to relax back to an axisymmetric state on an advective time scale, exhibiting a long-time weakening after many disturbance and relaxation cycles. The final axisymmetrization is a result of both advection and diffusion, but diffusion alone is insufficient to account for the degree of weakening. This relaxation process is often referred to as vortex axisymmetrization, and many studies have tried to capture its underlying dynamics. Melander *et al.* (1987) developed a descriptive framework to explain the vortex axisymmetrization process. They showed that elliptical vortices have nonzero potential vorticity located outside the saddle points in the co-rotating streamfunction, causing the potential vorticity to be pulled away from the vortex and filamented, leaving behind a smaller circular vortex. Montgomery and Kallenbach (1997) showed that vorticity perturbations on smooth-shaped, monopolar vortices propagate outward as Vortex Rossby Waves (VRWs) that are azimuthally sheared

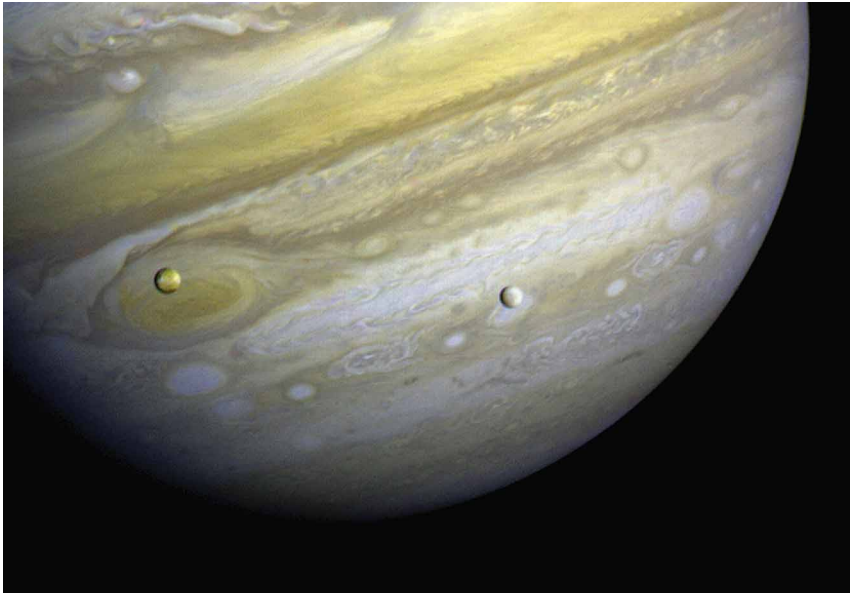


Figure 1. Jupiter's long-lived anticyclonic vortices visible as pale ovals. This photograph is from Voyager I on 13 February 1979. The moons Io (left) and Europa are also visible, and the Great Red Spot vortex lies behind Io (NASA/JPL).

by the differential angular velocity of the mean axisymmetric vortex. These fluctuations eventually transfer their energy back to the mean vortex, thereby strengthening it relative to the initial azimuthal mean flow. In a complementary study, Schecter *et al.* (2000) demonstrated some circumstances where energy exchange occurs between a fluctuation, sometimes referred to as a quasi-mode (Briggs *et al.* 1970), and the mean vortex at a critical radius where the azimuthal wave speed of the fluctuation equals the angular speed of the vortex.

To further understand the robustness of vortices, Bassom and Gilbert (1999; hereafter BG99), examined how a barotropic vortex, with a smooth radial vorticity profile responds to an external strain flow that is impulsive in time, has an extended duration, or is somewhat random. They analyzed the weakening of the azimuthal-mean vortex during the straining period and the subsequent relaxation of the vortex back to an axisymmetric state. They found that the net effect of an external strain flow is a weakening of the original vortex.

In this article we further explore this phenomenon using the Shallow-Water Equations (SWEs) with small but finite Rossby and Froude numbers (i.e., $Ro = V/fL$, where V and L are vortex azimuthal velocity and radial length scales, and f is the Coriolis frequency; $Fr = V/\sqrt{gH}$, where g is the gravitational acceleration, and H is the resting depth of the fluid layer). A striking characteristic of coherent vortices — not yet well understood — is the fact that, with finite Ro and deformation radius (i.e., $L_d = \sqrt{gH}/f$), anticyclones tend to be more prevalent than cyclones in flows that are not strongly influenced by horizontal or vertical boundaries. (This is in contrast with the development of stronger cyclones in baroclinic flows dominated by boundary potential temperature gradients, e.g., synoptic winter cyclones in the atmosphere.) Many studies have noted the preferential existence of anticyclones both in nature (e.g., atmospheric blocking anticyclones and submesoscale coherent vortices in the oceanic interior; McWilliams 1985) and in computational solutions of the SWE or its balanced approximation (Cushman-Roisin and Tang 1990, Arai and Yamagata 1994, Polvani *et al.* 1994, Cho and Polvani 1996) or in a fully three-dimensional (3D) flow (Yavneh *et al.* 1997). Whether there is a discrepancy in the number of emerging vortices with anticyclonic vorticity versus cyclonic vorticity, whether cyclones are more susceptible to an instability, or whether anticyclones are more robust to externally induced disturbances are all issues of continuing investigation.

Cushman-Roisin and Tang (1990) showed a preferential emergence of anticyclones from a random vorticity field when characteristic sizes were larger than L_d . They suggested this was due to an inherent tendency of cyclones to self-destruct. They proposed that the quadratic component of the planetary β -effect in their model is responsible for balancing Rossby-wave dispersion in anticyclones, akin to a soliton solution (cf Matura and Yamagata 1982). Cyclones, on the other hand, would fail to remain coherent since no such dynamical balance is possible. They also advanced a heuristic stability argument favoring anticyclone survival. However, since anticyclonic dominance has also been observed on an f -plane (e.g., Polvani *et al.* 1994), this β -dispersion argument cannot be the generic explanation.

Arai and Yamagata (1994) also observed anticyclonic dominance in numerically simulated flows when Ro is sufficiently large. To explain the phenomenon, they examined the problem of elliptical vortices on an f -plane. Anticyclonic ellipses were observed to undergo the familiar axisymmetrization process, regardless of the magnitude of Ro or L_d/L . In contrast, cyclonic ellipses elongated and eventually split

into two vortices. This tendency to elongate and split decreases as the ratio L_d/L decreases (see their figure 8). They suggested that this is the mechanism for anticyclonic dominance and remarked that vortex splitting is associated with the development of additional saddle points in the co-rotating streamfunction near the vortex core that implies an advective tendency to pull the vortex apart. We show that anticyclonic dominance does not require vortex splitting. To identify flow regimes displaying anticyclonic dominance, Polvani *et al.* (1994) performed numerical simulations of the SWE for the unforced evolution of initially random vorticity fields with a wide range of Ro and Fr values. They found that as Fr ($= Ro L/L_d$) increases at fixed Ro , so does the negative value of vorticity skewness, implying increased anticyclonic dominance. This is in apparent contradiction with the tendency favoring the occurrence of vortex splitting (Arai and Yamagata 1994). In order to reconcile this discrepancy, either initial condition differences are important (e.g., whether or not the vortices have zero circulation) or the interpretation that cyclonic elongation and splitting are the unique cause of anticyclonic dominance is incorrect.

Linear stability studies for vortices have, for the most part, failed to find a greater instability for cyclones. There are two finite- Ro instabilities, centrifugal (Charney 1973, Hoskins 1974) and ageostrophic anticyclonic (Molemaker *et al.* 2004), that imply greater anticyclonic instability. An exception is the study by Stegner and Dritschel (2000) that considered the instability and finite amplitude-evolution of zero-circulation vortices. Although they show a greater cyclonic growth rate of instability compared to anticyclones, the instability is essentially a quasi-geostrophic, inflection-point type, with only modest differences in evolution arising between cyclones and anticyclones with increasing Ro and increasing sharpness of the radial vorticity profiles. Therefore, we believe that linear stability behaviors are an insufficient explanation for the preferential persistence of anticyclones observed in interior flow regimes where many, if not most, vortices have nonzero circulation. Many different radial profile shapes arise for vortices in complex flows, and by their survival they are evidently stable.

Cho and Polvani (1996) showed that geostrophic adjustment by inertia-gravity wave radiation in the SWE favors stronger end-state anticyclones at intermediate Ro values, and Yavneh and McWilliams (1994) showed that, in the core of strongly deformed cyclones when the fluid depth approaches zero in the SWE, the dynamical approximation of diagnostic force balance breaks down, which instigates an enhanced dissipation rate. While both of these processes may contribute to anticyclonic dominance in general, neither is relevant to the essential phenomenon that occurs in balanced vortex dynamics.

In this article we present a new theory for the cause of anticyclonic dominance in large-scale geophysical flows, based on the demonstration that anticyclones are more robust than cyclones to perturbative disturbances at finite Ro . The theory's ingredients are the diagnostic force balances for the azimuthally averaged vortex and its asymmetric fluctuations (*balanced dynamics*); a linearized approximation for the fluctuation dynamics in the presence of the mean vortex; and a fully nonlinear representation of the azimuthally averaged momentum and mass fluxes by the fluctuations (*quasi-linear, eddy-mean interaction*; e.g., Lindzen and Holton 1968). Thus, the theory does not consider extreme finite-amplitude events, such as vortex splitting and filament expulsion (e.g., Nof 1990, 1991, Arai and Yamagata 1994, Drijfhout 2003) that we find not to be essential for the generic evolutionary behavior.

One way to describe the disturbance of any particular vortex in a complex, turbulent flow is to view the external influences as a time-varying strain flow acting on that vortex[†]. As shown in BG99, a strained barotropic vortex undergoes an initial weakening followed by an incomplete recovery to axisymmetry, resulting in a net weakening. We show that the essential difference between cyclones and anticyclones is in their response to such an external strain, whereby cyclones exhibit greater net weakening[‡].

Section 2 is the model derivation for the influence of an external strain flow on a vortex initially in axisymmetric, gradient-wind, and hydrostatic balance. Section 3 poses our specific problems and describes the numerical methods employed. Section 4 is a preview of the essential phenomena. Section 5 analyzes the weakening of a vortex during the impulsive straining period. Section 6 describes the strengthening of a vortex as it recovers from the external strain through VRW evolution. Section 7 presents the sensitivities to different parameters, such as strain duration, Ro and Fr, and advective nonlinearity of the fluctuations. Section 8 examines solutions when the external strain flow is sustained in time. Finally, section 9 provides a summary of the study and a discussion of remaining issues.

2. Dynamical model

We investigate the effect of a specified external, large-scale, straining flow on an initially axisymmetric, balanced vortex. The strain excites an asymmetric perturbation in the vortex that subsequently relaxes towards axisymmetry after the strain abates. We use the conservative, rotating SWE with a free upper surface and flat, solid bottom surface. In cylindrical coordinates (r, λ, t) , the primary dependent variables are the radial and azimuthal velocity (u, v) and geopotential ϕ . In a companion article (McWilliams *et al.* 2003; hereafter MGM03), the model equations are fully developed in the context of VRW solutions and their interaction with the mean vortex. Here, more briefly we record the relevant equations extended to include an external strain flow.

We decompose the primary variables with an ordering parameter, ϵ , that measures the relative sizes of the vortex fluctuation and external strain rate compared to the undisturbed vortex:

$$\begin{aligned} u &= \epsilon u'_i + \epsilon^2 \langle u_i \rangle + \epsilon u'_e + \epsilon^2 \langle u_e \rangle \\ v &= \bar{v}(r) + \epsilon v'_i + \epsilon^2 \langle v_i \rangle + \epsilon v'_e + \epsilon^2 \langle v_e \rangle \\ \phi &= \bar{\phi}(r) + \epsilon \phi'_i + \epsilon^2 \langle \phi_i \rangle + \epsilon \phi'_e + \epsilon^2 \langle \phi_e \rangle. \end{aligned} \quad (1)$$

[†]Earlier work by Brickman and Ruddick (1990) examined the instability of anticyclonic vortices to a barotropic straining flow. While the setup is similar to the problem solved here, they *did* not consider the comparative cyclonic case as we do here, and their model was restricted to vortices with a discontinuous potential-vorticity distribution (i.e., an anticyclonic ‘lens’) rather than the continuous profiles analyzed here.

[‡]Fully nonlinear simulations in 3D by Graves (2005) examining free-decay turbulence, vortex axisymmetrization, and vortex merger at finite Rossby number strongly support the paradigm of strain-weakening/relaxation-strengthening/anticyclonic-dominance developed here by our semi-analytical analysis.

The overbar denotes the initial vortex that is a stationary state in the absence of external strain. The primes and brackets denote azimuthally asymmetric and symmetric parts of the strain-induced flow. The subscripts e and i refer to the ‘external’ strain flow and ‘internal’ vortex perturbation, respectively. The $\langle \cdot \rangle$ and \cdot'_i quantities are referred to as the vortex changes and fluctuations. Note that we have subtracted off any bulk external velocity (e.g., evaluated at the vortex center, $r=0$), which only induces a bulk displacement of the vortex, to focus on the vortex deformation induced by the external velocity gradients across the vortex. The azimuthally averaged part of the external strain flow is an order smaller than the asymmetric part.

Inserting (1) into the SWE and separating by powers in ϵ , we obtain at $\mathcal{O}(\epsilon^0)$ the stationary gradient-wind balance for \bar{v} and $\bar{\phi}$,

$$\frac{d\bar{\phi}}{dr} = f\bar{v} + \frac{\bar{v}^2}{r}, \quad (2)$$

and at $\mathcal{O}(\epsilon)$ a linear SWE system for the fluctuations,

$$\begin{aligned} \bar{D}u'_i - \bar{\xi}v'_i &= -\partial_r\phi'_i + \bar{\Omega}(2v'_e - \partial_\lambda u'_e) \\ \bar{D}v'_i + \bar{\eta}u'_i &= -\frac{1}{r}\partial_\lambda\phi'_i - \bar{\zeta}u'_e - \bar{\Omega}\partial_\lambda v'_e \\ \bar{D}\phi'_i + g\bar{h}\delta'_i + u'_i\partial_r\bar{\phi} &= -g\bar{h}\delta'_e - \bar{\Omega}\partial_\lambda\phi'_e - u'_e\partial_r\bar{\phi}. \end{aligned} \quad (3)$$

There are no terms related to the external flow by itself since it is assumed to satisfy its own dynamical balance equations in the absence of the vortex. Relevant quantities are defined by

$$\begin{aligned} \bar{D} &= \partial_t + \frac{\bar{v}}{r}\partial_\lambda, \quad \bar{\Omega} = \frac{\bar{v}}{r}, \quad \bar{\zeta} = \frac{1}{r}\partial_r(r\bar{v}), \\ \bar{\eta} &= f + \bar{\zeta}, \quad \bar{\xi} = f + 2\bar{\Omega}, \quad \bar{h} = H + \frac{\bar{\phi}}{g}, \\ \bar{q} &= \frac{\bar{\eta}}{\bar{h}}, \quad \bar{\gamma}^2 = \frac{\bar{\eta}\bar{\xi}}{g\bar{h}}, \quad \delta' = \frac{1}{r}\partial_r(ru') + \frac{1}{r}\partial_\lambda v', \end{aligned} \quad (4)$$

where $\bar{\Omega}$ is the angular velocity of the vortex; \bar{D} is the substantial time derivative associated with advection by the mean vortex; $\bar{\zeta}$ is its relative vorticity; $\bar{\eta}$ is its absolute vorticity; $\bar{\xi}$ is twice its absolute rotation rate; \bar{h} is its layer depth; \bar{q} is its potential vorticity; $\bar{\gamma}^{-1}$ is its local deformation radius ($\sim L_d$); and δ' is the asymmetric component of horizontal divergence.

To exclude the fast inertia-gravity wave oscillations in (3), we make an approximation based on diagnostic force balance (McWilliams 2003), specifically the Asymmetric Balance (AB) approximation of Shapiro and Montgomery (1993) appropriate to nearly axisymmetric baroclinic flows[†] (assured here by $\epsilon \ll 1$). AB involves an iterative substitution for the velocity in the momentum equations in (3),

[†]The accuracy of AB solutions relative to the hydrostatic Primitive Equations for vortex flows has been well tested (e.g., by Moller and Montgomery (1999) and Schecter and Montgomery (2003) for vortices with finite L_d). AB becomes inaccurate in the barotropic limit at finite Ro, and we avoid its use in this situation.

starting from a generalized geostrophic balance in the first iterate (i.e., equating the second left-side and first right-side terms in the first two equations). After the next iteration, the result is

$$\begin{aligned} u'_i &= -\frac{1}{\bar{\eta}} \left[\frac{1}{r} \partial_\lambda \phi'_i + \frac{1}{\bar{\xi}} \bar{D}(\partial_r \phi'_i) + \bar{\zeta} u'_e + \bar{\Omega} \partial_\lambda v'_e \right] \\ v'_i &= \frac{1}{\bar{\xi}} \left[\partial_r \phi'_i - \frac{1}{\bar{\eta} r} \bar{D}(\partial_\lambda \phi'_i) + \bar{\Omega}(\partial_\lambda u'_e - 2v'_e) \right]. \end{aligned} \quad (5)$$

Substituting (5) into the continuity equation[†] in (3) and multiplying everything by $-\bar{\gamma}^2$, we get the fluctuation geopotential tendency equation (cf MGM03):

$$\begin{aligned} \bar{D}[q^{ab}] - \frac{1}{r} \bar{G} \partial_\lambda \phi'_i &= -\bar{\eta} \bar{\xi} \left[\frac{1}{r} \partial_r \left(\frac{r}{\bar{\eta}} (\bar{\zeta} u'_e + \bar{\Omega} \partial_\lambda v'_e) \right) + \frac{\bar{\Omega}}{r \bar{\xi}} (2 \partial_\lambda v'_e - \partial_\lambda^2 u'_e) - \delta'_e \right] \\ &\quad + \bar{\gamma}^2 \left[\frac{\partial_r \bar{\phi}}{\bar{\eta}} (f u'_e - \bar{\Omega} \partial_\lambda v'_e) + \bar{\Omega} \partial_\lambda \phi'_e \right], \end{aligned} \quad (6)$$

where

$$q^{ab} = \bar{\nabla}^2 \phi'_i - \bar{\gamma}^2 \phi'_i, \quad \bar{G}(r) = \bar{\xi} \partial_r [\ln \bar{\eta}], \quad \bar{\nabla}^2 = \frac{\bar{\gamma}^2}{r} \partial_r \left(\frac{r}{\bar{\gamma}^2} \partial_r \right) + \frac{1}{r^2} \partial_\lambda^2. \quad (7)$$

q^{ab} is the fluctuation potential vorticity in the AB approximation. All fluctuation (primes) and vortex change terms (brackets) are initially zero, as is the external strain (section 3). The boundary conditions for ϕ'_i , and thus for $\partial_t \phi'_i$, are zero for both itself and its radial derivative at $r=0$, and decay $\sim r^{-2}$ at the outer boundary due to the choice for the external strain flow (section 3) or even more steeply $\sim e^{-r/L_d}$ after the strain abates.

Inserting (1) into the SWE and azimuthally averaging, we obtain at $\mathcal{O}(\epsilon^2)$ beyond (2) the following system for the vortex changes:

$$\begin{aligned} \partial_t \langle u_i \rangle - \bar{\xi} \langle v_i \rangle &= -\partial_r \langle \phi_i \rangle - \langle \Sigma N^u \rangle + 2 \bar{\Omega} \langle v_e \rangle \\ \partial_t \langle v_i \rangle + \bar{\eta} \langle u_i \rangle &= -\langle \Sigma N^v \rangle - \bar{\zeta} \langle u_e \rangle \\ \partial_t \langle \phi_i \rangle + \frac{1}{r} \partial_r (r g \bar{h} \langle u_i \rangle) &= -\langle \Sigma N^\phi \rangle - \frac{1}{r} \partial_r (r g \bar{h} \langle u_e \rangle), \end{aligned} \quad (8)$$

[†]As discussed in MGM03, there is an alternative derivation for the AB asymmetric geopotential tendency equation, where the velocity approximations (5) are substituted into the linearized asymmetric potential-vorticity equation. The two alternatives for the AB approximation are referred to as the continuity path and potential-vorticity path, respectively. The paths are of an equivalent formal order of accuracy in Ro , with errors $\mathcal{O}((|\bar{D}|/f)^2)$, but they differ in several of their higher-order terms. We have examined solutions to the strain/relaxation problem (sections 4 and 5) using both paths; they differ only modestly at larger values of Ro , and their qualitative behaviors are the same. The potential-vorticity path has an additional complexity in the strain-impulse limit (section 5), where its solution is divergent as $f_{max} \rightarrow 0$ (a limit that is formally inappropriate for balanced dynamics anyway), although it is well behaved as long as $Ro^{-1} > f_{max} \geq 1$. In this report, for simplicity we do not show results from the potential-vorticity path. It is a common experience (McWilliams 2003) that alternative balance approximations give modestly, but not importantly, different answers in the regime of intermediate Ro where they are most relevant.

where the quadratic advection terms due to the fluctuations are defined by

$$\Sigma N^u = \left\{ \begin{array}{l} u'_i \partial_r u'_i + \frac{1}{r} v'_i \partial_\lambda u'_i - \frac{1}{r} (v'_i)^2 \\ + u'_i \partial_r u'_e + \frac{1}{r} v'_i \partial_\lambda u'_e - \frac{1}{r} v'_i v'_e \\ + u'_e \partial_r u'_i + \frac{1}{r} v'_e \partial_\lambda u'_i - \frac{1}{r} v'_e v'_i \end{array} \right\} \quad (9)$$

$$\Sigma N^v = \left\{ \begin{array}{l} u'_i \partial_r v'_i + \frac{1}{r} v'_i \partial_\lambda v'_i + \frac{1}{r} u'_i v'_i \\ + u'_i \partial_r v'_e + \frac{1}{r} v'_i \partial_\lambda v'_e + \frac{1}{r} u'_i v'_e \\ + u'_e \partial_r v'_i + \frac{1}{r} v'_e \partial_\lambda v'_i + \frac{1}{r} u'_e v'_i \end{array} \right\} \quad (10)$$

$$\Sigma N^\phi = \left\{ \begin{array}{l} \frac{1}{r} \phi'_i \partial_r (r u'_i) + u'_i \partial_r \phi'_i + \frac{1}{r} \partial_\lambda (v'_i \phi'_i) \\ + \frac{1}{r} \phi'_i \partial_r (r u'_e) + u'_i \partial_r \phi'_e + \frac{1}{r} \partial_\lambda (v'_i \phi'_e) \\ + \frac{1}{r} \phi'_e \partial_r (r u'_i) + u'_e \partial_r \phi'_i + \frac{1}{r} \partial_\lambda (v'_e \phi'_i) \end{array} \right\}. \quad (11)$$

The fluctuation nonlinear terms in (8) are calculated by solving (6) for ϕ'_i , evaluating (5) for u'_i and v'_i , substituting into (9)–(11), and azimuthally averaging.

For the vortex changes we make a Gradient-wind Balance Equation (BE) approximation (MGM03) to exclude inertia-gravity oscillations. In (8) this is accomplished simply by dropping the radial acceleration term, $\partial_t \langle u_i \rangle$, in the first equation; hence, rearrangement yields

$$\begin{aligned} \langle u_i \rangle &= -\frac{1}{\bar{\eta}} [\partial_t \langle v_i \rangle + \langle \Sigma N^v \rangle + \bar{\zeta} \langle u_e \rangle] \\ \langle v_i \rangle &= \frac{1}{\bar{\xi}} [\partial_r \langle \phi_i \rangle + \langle \Sigma N^u \rangle - 2\bar{\Omega} \langle v_e \rangle]. \end{aligned} \quad (12)$$

Substituting (12) into the third equation of (8) and multiplying by $-\bar{\gamma}^2$ gives

$$\begin{aligned} \frac{\bar{\gamma}^2}{r} \partial_r \left(\frac{r}{\bar{\gamma}^2} \partial_r \partial_t \langle \phi \rangle \right) - \bar{\gamma}^2 \partial_t \langle \phi \rangle &= \bar{\gamma}^2 \langle \Sigma N^\phi \rangle - \frac{\bar{\gamma}^2}{r} \partial_r \left[\frac{r}{\bar{q}} \langle \Sigma N^v \rangle \right] - \bar{\Gamma} [\partial_t \langle \Sigma N^u \rangle] \\ &+ \frac{\bar{\gamma}^2}{r} \partial_r \left[2 \frac{r \bar{\Omega}}{\bar{\gamma}^2} \partial_t \langle v_e \rangle - \frac{r}{\bar{q}} \bar{\zeta} \langle u_e \rangle \right] + \frac{\bar{\gamma}^2}{r} \partial_r (r g \bar{h} \langle u_e \rangle), \end{aligned} \quad (13)$$

where the operator $\bar{\Gamma}$ is defined by

$$\bar{\Gamma}[Q] = \frac{\bar{\gamma}^2}{r} \partial_r \left[\frac{r}{\bar{\gamma}^2} Q \right]. \quad (14)$$

The initial conditions are zero for all bracketed quantities. The boundary conditions for $\langle \phi_i \rangle$ are $\partial_r \langle \phi_i \rangle = 0$ at $r=0$ and decay $\sim r^{-4}$ at the outer boundary for $\langle \phi_i \rangle$ due to the external strain (section 3) or even more steeply $\sim e^{-r/L_d}$ after the strain abates.

Equations (6) and (13) and their supporting relations comprise a well-posed initial- and boundary-value problem for the evolution of the fluctuations and vortex changes under the influence of a specified external flow. They have well-defined quasigeostrophic (QG) and barotropic (BT) dynamical limits obtained by $\text{Ro} \rightarrow 0$ and $L_d \rightarrow \infty$.

To assess whether the straining and relaxation processes weaken or strengthen the vortex, we evaluate norms based on the area integrals, of the total energy and potential enstrophy densities, viz.,

$$\mathcal{E}_{swe}[v, u, \phi] = \frac{1}{2} \left(h(u^2 + v^2) + \frac{1}{g} \phi^2 \right), \quad \mathcal{V}_{swe}[v, u, \phi] = \frac{1}{2} h q^2, \quad (15)$$

where $h = H + \phi/g$, $q = (f + \zeta)/h$, and $\zeta = r^{-1}(\partial_r[r v] - \partial_\lambda[u])$. Both of these norms are preserved during a conservative evolution for the vortex, although they are not conserved when the external strain flow is included. To assess the changes in the vortex, we subtract the initial values of the norm associated with the initial vortex (e.g., \bar{v} , etc.), and we either include the fluctuation components (e.g., v'_i , etc.) or not in evaluating (15) to distinguish between changes to the fluctuation part of the vortex perturbation or to only its azimuthally averaged part. For example, excluding the contributions from the external strain flow,

$$\Delta \bar{\mathcal{E}}_{swe}(t) = \mathcal{E}_{swe}[v_i = \bar{v} + \epsilon^2 \langle v_i \rangle(t), \text{etc.}] - \mathcal{E}_{swe}[v_i = \bar{v}, \text{etc.}] \quad (16)$$

is a measure of the energy change density that has occurred in the azimuthally averaged vortex structure, and

$$\Delta \mathcal{E}'_{swe}(t) = \mathcal{E}_{swe}[v = v_i = \bar{v} + \epsilon v'_i(t) + \epsilon^2 \langle v_i \rangle(t), \text{etc.}] - \mathcal{E}_{swe}[v = v_i = \bar{v} + \epsilon^2 \langle v_i \rangle(t), \text{etc.}] \quad (17)$$

measures the energy density in the fluctuations. We denote the area integrals of (16) and (17) by $\Delta \bar{\mathcal{E}}_{swe}$ and $\Delta \mathcal{E}'_{swe}$, respectively, and the analogous potential enstrophy change measures are $\Delta \bar{\mathcal{V}}_{swe}$ and $\Delta \mathcal{V}'_{swe}$.

3. Problem posing and computational method

The initial vortex is chosen to have a monotonic relative vorticity profile,

$$\bar{\zeta}(r) = \zeta_0 e^{-(r/r_0)^3}, \quad (18)$$

and thus a finite circulation (i.e., area integral vorticity). The constants, ζ_0 and r_0 , are chosen such that the associated swirl profile, $\bar{v}(r)$ from (4), has a maximum wind speed V at a radius of L . For definiteness in our primary cases, we choose $V = 4 \text{ m s}^{-1}$ and $L = 200 \text{ km}$. Along with $f = 10^{-4} \text{ s}^{-1}$, these values imply $\text{Ro} = V/fL = 0.2$, although a related quantity, $|\bar{\zeta}|(r=0)/f$ has a rather larger value of 0.7. The associated

geopotential $\bar{\phi}$ is calculated from (2) with an outer boundary condition of $\bar{\phi} = 0$ at $r = R_{max}$. We choose $R_{max} = 2000$ km after confirming in trial solutions of (6) and (13) that this is sufficiently distant for its specific value not to matter. The behavior shown below is not qualitatively sensitive to the particular profile choice in (18) (except perhaps in the limiting case of a step-function profile where critical-layer interactions and quasi-mode behaviors may become more prominent).

We choose the following as a canonical external strain flow that acts only over a limited time interval, $0 \leq t \leq t_{max}$:

$$u'_e = -\alpha F(t)r \cos[2\lambda], \quad v'_e = +\alpha F(t)r \sin[2\lambda], \quad \langle u_e \rangle = \langle v_e \rangle = 0, \quad (19)$$

where α is the strain rate and

$$F(t) = \sin^2 \left[\frac{\pi t}{t_{max}} \right], \quad 0 \leq t \leq t_{max} \\ = 0, \quad t \geq t_{max} \quad (20)$$

is its non-dimensional time history. The cumulative straining magnitude by (19)–(20) after t_{max} is

$$\int_0^{t_{max}} dt \alpha F(t) = \frac{\alpha t_{max}}{2} \equiv m, \quad (21)$$

and we choose $m \ll 1$ consistent with $\epsilon \ll 1$ in (1). This flow is zero at the vortex center, is non-divergent, and has zero vorticity. The associated external geopotential is

$$\phi'_e = \frac{\alpha f}{2} F(t)r^2 \sin[2\lambda], \quad \langle \phi_e \rangle = -\frac{1}{2}(\alpha Fr)^2, \quad (22)$$

which is in (r, λ) gradient-wind balance with (19). Again, the results we report are not particularly sensitive to the choice for (u_e, v_e) as long as its spatial scale is much larger than L .

As the centerpiece of this work, we focus on four primary cases: CYCLONE (with $\zeta_0 > 0$ in (18) and $\text{Ro} = 0.2$); ANTICYCLONE (with $\zeta_0 < 0$ in (18) and $\text{Ro} = 0.2$); QG (deleting all $\mathcal{O}(\text{Ro})$ contributions in (6) and (13)), which has equivalent solutions for either sign of ζ_0 though we do show results for a cyclonic case with $\zeta_0 > 0$; and BT (the same as QG except $L_d \rightarrow \infty$, hence $\bar{\gamma}^2 \rightarrow 0$, e.g., by taking the limit $H \rightarrow \infty$)[†], which is directly comparable with the solutions in BG99. For the non-barotropic cases the layer depth is chosen to be $H = 50$ m, which yields an L_d value of 220 km, close to the value of L and consistent with parameter regime surveyed by Cushman-Roisin and Tang (1990) and Polvani *et al.* (1994). The duration of the strain period is $t_{max} = 4500$ s (1.25 h); thus, it is of brief duration (i.e., impulsive)

[†]Barotropic dynamics has the same velocity evolution for all values of Ro . However, its associated geopotential field is in gradient-wind balance and thus depends on Ro . We choose $\text{Ro} \rightarrow 0$ for the BT case for direct comparability to the QG solution with finite L_d and so that ϕ/f is interpretable as the streamfunction.

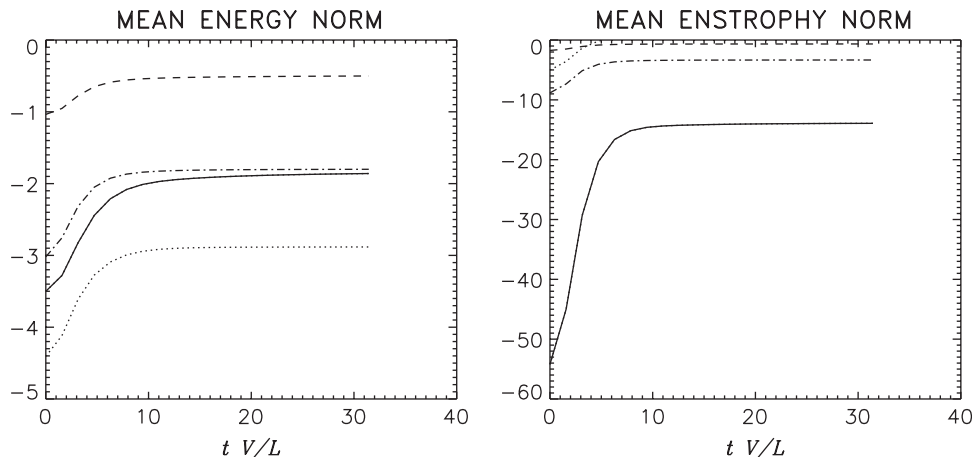


Figure 2. History of the normalized vortex change norms for (left) energy, $\Delta\bar{E}_{\text{swv}}(t)$, and (right) potential enstrophy, $\Delta\bar{E}'_{\text{swv}}(t)$, for the primary cases with impulsive strain: CYCLONE = solid line; ANTICYCLONE = long-dash line; QG = dash-dot line; and BT = dotted line. Normalizations are in table 1. All curves start at zero for $t=0$, but the strain-weakening period is so brief (i.e., $t_{\text{max}} V/L = 0.014$) on the scale of the plot that they appear to start at their post-strain, minimum values.

compared to the vortex advective turn-around time, $2\pi L/V \approx 3.6$ days, the characteristic time for VRW evolution (MGM03). We also choose a rather weak external strain rate, $\alpha = 10^{-7} \text{ s}^{-1}$, hence $m = 2 \times 10^{-4} \ll 1$. All of the primary cases are run for 5 eddy turn-around times (defined at the radius of maximum swirl velocity), by which point the VRW relaxation process has asymptotically approached its long-time limit in the sense that the energy and enstrophy norms are no longer changing significantly. In addition, other cases (defined in sections 6 and 7) are investigated to explore sensitivities in this primary problem formulation.

The numerical model used to solve the tendency equations for the geopotential is semi-spectral, with Fourier modes in the azimuthal coordinate and second-order, centered finite differences in the radial coordinate. The nonlinear terms are computed by explicitly summing a convolution sum in Fourier space. Inversion for the geopotential tendencies $\partial_t \phi'_i$ and $\partial_t (\phi_i)$ is accomplished with an LU-decomposition of a band-diagonal matrix derived from the elliptic operator in equations (6) and (16). The tendencies in the nonlinear terms on the right-hand side are used from the previous timestep. The numerical model is time-stepped with a fourth-order Runge-Kutta scheme. A time step of 100 s with a radial grid spacing of 5 km falls within the CFL computational stability threshold.

4. Strain-induced net weakening and anticyclonic dominance

The essential phenomenon is illustrated by the histories of the vortex change norms in the four primary cases (figure 2). Note that these are area integrals of the densities given in (15) and (16). In all cases, the azimuthally averaged energy and potential enstrophy decrease during the straining period ($0 < t < t_{\text{max}}$), and then they partially recover

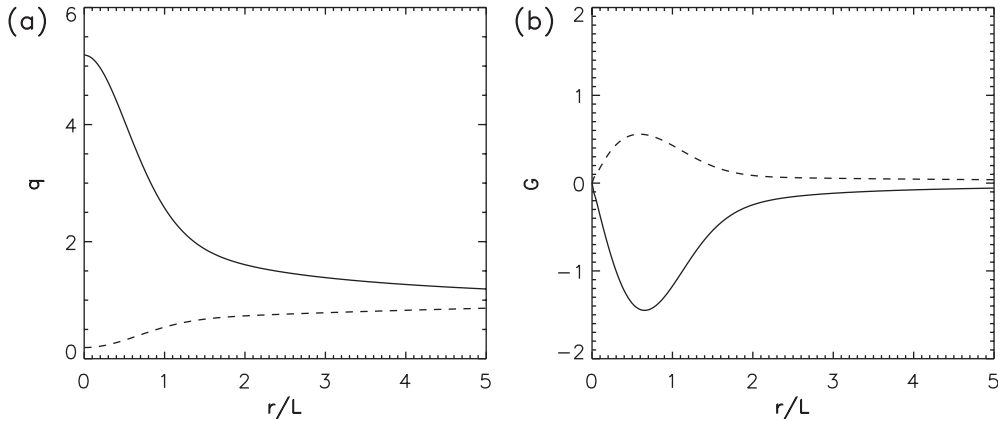


Figure 3. (a) $\bar{q}(r)$ normalized by f/gH and (b) $\bar{G}(r)$ normalized by f/L in CYCLONE (solid line) and ANTICYCLONE (dashed line).

during the relaxation period ($t_{max} < t < \infty$). These two periods are analyzed separately in sections 4 and 5. Note that the changes in the azimuthally averaged vortex are much larger in CYCLONE than those in ANTICYCLONE, with QG in between and BT outside their range.

In advance of the detailed analysis, we can give a simple heuristic rationalization for anticyclonic dominance. The external strain field will induce a displacement $\boldsymbol{\mu}'$ of vortex parcels away from their equilibrium position. This is a conservative process, in particular of potential vorticity. Within the vortex, the dominant potential vorticity is that of the mean vortex itself, $\bar{q}(r)$. Hence we expect potential vorticity fluctuations that can be estimated for small displacements as

$$q' \approx -\boldsymbol{\mu}' \cdot \hat{\mathbf{r}} \frac{d\bar{q}}{dr}.$$

Because of the combined nonlinearities in gradient-wind balance and potential vorticity for finite Ro , $d_r \bar{q}$ is very much larger for cyclones than anticyclones (figure 3a). Hence, for equal parcel displacements within the vortex, the q' fluctuations will be larger in cyclones. Hence the vortex changes driven by the fluctuations will be larger. Since the net change is weakening (figure 2), cyclones will be weakened more, and this provides an evolutionary path towards relatively stronger anticyclones. Note that this argument makes no specific reference to the governing equations or the vortex and external flow shapes; so we can further expect that the behavior analyzed here will occur under many different circumstances.

5. Vortex weakening by impulsive strain

To understand the mechanism of vortex weakening caused by an external strain flow, we solve an approximate problem for the vortex evolution when the straining event

has a short duration t_{max} compared to the free evolution of VRWs that occurs on the advective time scale L/V . The size of the net effect from (19) is measured by

$$M(t) = \frac{2m}{t_{max}} \int_0^t F(t') dt'. \quad (23)$$

M is zero at $t=0$, increases monotonically for all $t \geq 0$, and is equal to m defined in (21) for all $t \geq t_{max}$. Consistent with the approximation $\epsilon \ll 1$ (section 2), we assume that $0 < m \ll 1$, which implies a small-amplitude vortex perturbation by the external strain flow. The strain-impulse approximation is a finite-time version of the delta-function limit of impulsive strain (i.e., $t_{max} \rightarrow 0$, $\alpha \rightarrow \infty$, and m finite), and its solution is the same for all times $L/V \gg t \geq t_{max}$. More generally the external strain flow can have its duration time t_{max} be either comparable to or longer than the vortex Rossby-wave time (cf sections 6 and 7). The processes of strain-induced weakening and wave-induced recovery (section 6) will then occur simultaneously and with mutual interaction. Nevertheless, the most useful paradigm for strain-induced weakening is the response of a stationary vortex to an impulsive external strain flow.

The impulsive-strain approximation allows us to neglect the VRW propagation terms proportional to $\bar{\Omega}$ and \bar{G} on the left side of (6). With a plane-strain external flow (19), the fluctuation equation is

$$\left[\tilde{\nabla}^2 - \bar{\gamma}^2 \right] \frac{\partial \phi'}{\partial t} = \dot{M}(t) \cos[2\lambda] \left[\frac{\bar{\eta} \bar{\xi}}{r} \frac{\partial}{\partial r} \left[\frac{r^2 \bar{S}}{\bar{\eta}} \right] + \bar{\gamma}^2 \frac{f \bar{\nu} r}{\bar{\eta}} \left(\bar{\eta} - \bar{\xi} \left(1 + \frac{\bar{\Omega}}{f} \right) \right) \right], \quad (24)$$

with $\bar{S} = rd_r[\bar{\nu}/r]$ the strain flow for the mean vortex and \dot{M} the time derivative of $M(t)$. The solution of (24) has a separable form,

$$\phi'(r, \lambda, t) = M(t) \cos[2\lambda] \hat{\phi}'(r), \quad (25)$$

with $\hat{\phi}'(r)$ determined from (24) after substituting (25) and factoring out the (λ, t) dependences (i.e., the resulting right-side forcing is the term within the outer brackets). In the more easily interpreted QG limit ($Ro \rightarrow 0$), the $\hat{\phi}'(r)$ equation simplifies to

$$\left[\frac{1}{r} \frac{d}{dr} \left(r \frac{d}{dr} \right) - \left(\frac{4}{r^2} + L_d^{-2} \right) \right] \hat{\phi}' = \frac{f}{r} \frac{d}{dr} [r^2 \bar{S}]. \quad (26)$$

The right-side forcing in (26) vanishes as $r \rightarrow 0, \infty$, and it has a single extremum in between. For finite Ro values the more general right-side forcing in (24) has a qualitatively similar shape. The strain-induced fluctuation (25) grows monotonically with an azimuthal pattern in quadrature with the strain flow's (22). The overall magnitude of ϕ' is $\mathcal{O}(mfVL)$.

The radial structure function for the fluctuations $\hat{\phi}'(r)$ is shown in figure 4 for the standard cases in section 3. It has the shape of a single dominant extremum

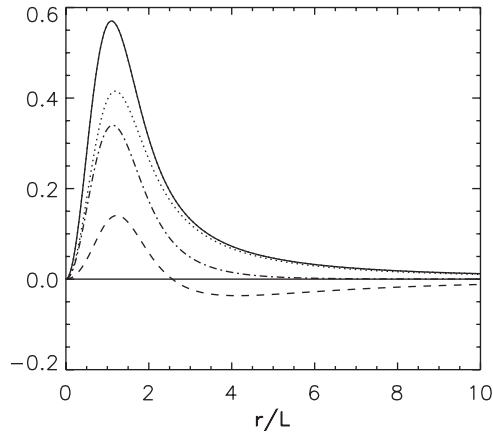


Figure 4. $\hat{\phi}'(r)$, defined in (25) and normalized by VfL , for the primary cases defined in section 3: CYCLONE = solid line; ANTICYCLONE (with the sign reversed) = long-dash line; QG = dash-dot line; BT = dot line. The radius is normalized by L .

just beyond the radius of maximum vortex velocity, consistent with the shape of \bar{S} in (26). Compared to the QG solution, the CYCLONE solution has a much stronger fluctuation amplitude, and the ANTICYCLONE solution has a much weaker one. These tendencies are a simple consequence of the larger magnitudes of $\bar{\eta}/f$, $\bar{\xi}/f$, and $L_d^2 \bar{\gamma}^2$ in CYCLONE amplifying the right-side in (24) and their smaller values diminishing the right-side in ANTICYCLONE. Furthermore, the two groups of forcing terms on the right side of (24) are additive for cyclones with finite Ro , and they have opposing signs for anticyclones; this further accentuates the reduction in the net forcing magnitude. These forcing differences imply that external straining disrupts cyclones more substantially than anticyclones as Ro increases, through the advective interaction of the external strain flow and the mean vortex. It is interesting that $\hat{\phi}'(r)$ (hence also q^{ab}) changes sign in the outer region for ANTICYCLONE; this will prove to be significant in the response to sustained strain (section 8). Finally, $\hat{\phi}'(r)$ is modestly larger in the BT solution, compared to QG; both solutions have the same right-side forcing in (26), but BT has a larger fluctuation response (i.e., ϕ/q ratio) than QG since it lacks the vortex-stretching term $\propto L_d^{-2}$ in q .

The vortex change equation (13) has a composite separable solution form, viz.,

$$\langle \phi \rangle(r, t) = M^2(t) \langle \hat{\phi} \rangle_M(r) + \frac{\dot{M}^2(t)}{f^2} \langle \hat{\phi} \rangle_{\dot{M}}(r). \quad (27)$$

Its first term is $\mathcal{O}(m^2 fVL)$, and it exhibits monotonic growth until $t = t_{max}$ after which it is steady. Its second term is $\mathcal{O}(m^2 fVL/(ft_{max})^2)$. It is at least as large as the first one in the impulsive-strain limit, but its temporal structure is a single-signed pulse in the interval between vanishing at $t=0$ and $t \geq t_{max}$. Thus, the second term represents a fully reversible response during the straining event, and the persistent vortex change caused by straining is entirely represented by the first term, $\langle \hat{\phi} \rangle_M$.

Consistent with the solution form (27), we decompose the fluctuation nonlinear terms in (13) as follows:

$$\begin{aligned}
\langle \Sigma N^\phi \rangle &= \frac{1}{f} \frac{dM^2}{dt}(t) \mathcal{N}^\phi(r), \\
\mathcal{N}^\phi &= -\frac{f}{4r} \frac{d}{dr} \left[\frac{r^2 \hat{\phi}'}{\bar{\eta}} \left(2\bar{\Omega} + \frac{1}{\bar{\xi} r} \frac{d\hat{\phi}'}{dr} \right) - \frac{f \bar{\Omega} r^3}{\bar{\eta} \bar{\xi}} \frac{d\hat{\phi}'}{dr} \right]; \\
\langle \Sigma N^u \rangle &= M^2(t) \mathcal{N}_M^u(r) + \frac{\dot{M}^2}{f^2}(t) \mathcal{N}_{\dot{M}}^u(r), \\
\mathcal{N}_M^u &= \frac{d}{dr} \left[\frac{1}{\bar{\eta}^2 r^2} \left(\frac{\bar{\Omega} r}{\bar{\xi}} \frac{d\hat{\phi}'}{dr} + \hat{\phi}' \right)^2 \right] - \frac{1}{2\bar{\xi}^2 r} \left(1 - \frac{4\bar{\Omega}}{\bar{\eta}} \right) \left(\frac{d\hat{\phi}'}{dr} \right)^2 \\
&\quad + \frac{8\bar{\Omega}}{\bar{\eta}^2 \bar{\xi} r^3} \left(1 - \frac{\bar{\Omega}}{\bar{\xi}} \right) \hat{\phi}'^2 + \frac{2}{\bar{\eta} \bar{\xi} r^2} \left(1 - \frac{2\bar{\Omega}}{\bar{\xi}} + \frac{4\bar{\Omega}^2}{\bar{\eta} \bar{\xi}} \right) \hat{\phi}' \frac{d\hat{\phi}'}{dr}, \\
\mathcal{N}_{\dot{M}}^u &= -\frac{f^2}{2} \frac{d}{dr} \left[\frac{r}{\bar{\eta}} \left(r\bar{S} - \frac{1}{\bar{\xi}} \frac{d\hat{\phi}'}{dr} \right) \left(1 - \frac{\bar{S}}{2\bar{\eta}} + \frac{1}{2\bar{\eta} \bar{\xi} r} \frac{d\hat{\phi}'}{dr} \right) \right] \\
&\quad - \frac{f^2}{\bar{\eta}} \left[\left(r\bar{S} - \frac{1}{\bar{\xi}} \frac{d\hat{\phi}'}{dr} \right) \left(1 + \frac{2\hat{\phi}'}{\bar{\eta} \bar{\xi} r^2} \right) + \frac{2\hat{\phi}'^2}{\bar{\eta} \bar{\xi}^2 r^3} \right]; \\
\langle \Sigma N^v \rangle &= \frac{1}{f} \frac{dM^2}{dt}(t) \mathcal{N}^v(r), \\
\mathcal{N}^v &= -\frac{f}{\bar{\eta}} \left(\bar{\eta} - \bar{S} + \frac{1}{\bar{\xi} r} \frac{d\hat{\phi}'}{dr} \right) \left(\frac{1}{4} \frac{d}{dr} \left[\frac{r}{\bar{\xi}} \frac{d\hat{\phi}'}{dr} \right] + \frac{\bar{S} \hat{\phi}'}{\bar{\eta} \bar{\xi} r} \right) \\
&\quad + \frac{f}{\bar{\eta}} \left(\frac{\hat{\phi}'}{r^2} - \bar{\Omega}(\bar{\eta} - \bar{S}) \right) \frac{d}{dr} \left[\frac{\hat{\phi}'}{\bar{\eta} \bar{\xi}} \right] + \frac{f}{\bar{\eta} r} \left(\frac{\bar{\Omega} r}{\bar{\xi}} \frac{d\hat{\phi}'}{dr} + \hat{\phi}' \right). \tag{28}
\end{aligned}$$

The resulting radial boundary value problems for the components of $\langle \phi \rangle$ in (27) are

$$\begin{aligned}
\left[\frac{1}{r} \frac{d}{dr} \left(\frac{r}{\bar{\gamma}^2} \frac{d}{dr} \right) - 1 \right] \langle \hat{\phi} \rangle_M &= \frac{1}{f} \mathcal{N}^\phi - \frac{1}{r} \frac{d}{dr} \left[\frac{r \mathcal{N}^v}{f \bar{\gamma}} + \frac{r \mathcal{N}_M^u}{\bar{\gamma}^2} \right] \\
\left[\frac{1}{r} \frac{d}{dr} \left(\frac{r}{\bar{\gamma}^2} \frac{d}{dr} \right) - 1 \right] \langle \hat{\phi} \rangle_{\dot{M}} &= -\frac{1}{r} \frac{d}{dr} \left[\frac{r \mathcal{N}_{\dot{M}}^u}{\bar{\gamma}^2} \right]. \tag{29}
\end{aligned}$$

The velocities for the vortex change (12) have an analogous decomposition into

$$\begin{aligned}
\langle u \rangle &= \frac{1}{f} \frac{dM^2}{dt}(t) \langle \hat{u} \rangle_M(r) + \frac{1}{f} \frac{d}{dt} \left[\frac{\dot{M}^2(t)}{f^2} \right] \langle \hat{v} \rangle_{\dot{M}}(r) \\
\langle v \rangle &= M^2(t) \langle \hat{v} \rangle_M(r) + \frac{\dot{M}^2(t)}{f^2} \langle \hat{v} \rangle_{\dot{M}}(r). \tag{30}
\end{aligned}$$

The resulting relations for their radial functions are

$$\begin{aligned}\langle \hat{u} \rangle_j &= -\frac{1}{\xi} (f \langle \hat{v} \rangle_j + \delta_{j,M} \mathcal{N}^v), \\ \langle \hat{v} \rangle_j &= \frac{1}{\xi} \left(\frac{d \langle \hat{\phi} \rangle_j}{dr} + \mathcal{N}_j^u \right)\end{aligned}\quad (31)$$

for $j = M, \dot{M}$ and $\delta_{j,j}$ the discrete delta function (i.e., $\delta = 1$ for equal indices and $\delta = 0$ otherwise). The vortex change velocity magnitudes are $\mathcal{O}(m^2 V / (ft_{max}))$ and $\mathcal{O}(m^2 V / (ft_{max})^3)$, respectively, for the two $\langle u \rangle_j$ components in (30), and they are $\mathcal{O}(m^2 V)$ and $\mathcal{O}(m^2 V / (ft_{max})^2)$, respectively, for the two $\langle v \rangle_j$ components. They are all small compared to \bar{v} by the factor m^2 , and they are enhanced in magnitude during the strain-impulse phase by various factors of $1/(ft_{max})$. After the strain impulse has ended (i.e., for $t \geq t_{max}$), the only nonzero velocity component is $\langle v \rangle_M$ with a magnitude of $\mathcal{O}(m^2 V)$.

In the QG case, $\mathcal{N}^\phi = \mathcal{N}_M^u = 0$, and \mathcal{N}_M^u , although nonzero, does not contribute to the leading-order relations for $\langle \phi \rangle_M$, $\langle u \rangle$, and $\langle v \rangle$. The limiting form for (29) is

$$\left[\frac{1}{r} \frac{d}{dr} \left(r \frac{d}{dr} \right) - L_d^{-2} \right] \langle \hat{\phi} \rangle_M = -\frac{1}{r} \frac{d}{dr} [r \mathcal{N}^v], \quad (32)$$

with the eddy momentum flux forcing,

$$\mathcal{N}^v = \frac{\hat{\phi}'}{r} - \frac{1}{4} \frac{d}{dr} \left[r \frac{d \hat{\phi}'}{dr} \right]. \quad (33)$$

The associated QG velocity components are

$$\langle \hat{u} \rangle = 0, \quad \langle \hat{v} \rangle = \frac{1}{f} \frac{d \langle \hat{\phi} \rangle_M}{dr}. \quad (34)$$

The radial structures that survive at the end of the strain-impulse period, $\langle \hat{\phi} \rangle_M$ and $\langle \hat{v} \rangle_M$, are shown in figure 5 for the standard cases in section 3. Their profiles are generally similar among the cases. $\langle \phi \rangle / f$ is positive within the vortex core, opposite to the sign of $\bar{\phi} / f$. $\langle v \rangle$ is also opposite in sign to \bar{v} near its extremum at $r = L$. These indicate a weakening of the vortex during the straining event. The magnitudes of the vortex change profiles are larger for CYCLONE than ANTICYCLONE and smaller for QG than for BT.

The dominant forcing term for $\langle \hat{\phi} \rangle_M$ in (29) is \mathcal{N}^v , and its largest components are those analogous to the QG ones in (33). The dominance of these terms also occurs for $\langle v \rangle$ in (31). The principal source of cyclone–anticyclone differences is the $\mathcal{O}(\text{Ro})$ forcing terms involving the advective interaction of the external strain flow, the mean vortex, and the strain-induced fluctuation, ϕ' (i.e., not those involving quadratic products of the fluctuations nor those of $\mathcal{O}(\text{Ro}^2)$). For example, a member of the important $\mathcal{O}(\text{Ro})$ class of terms in \mathcal{N}^v in (28) is $-\bar{S} \hat{\phi}' / \bar{\eta} \xi r$. In the case of cyclones these extra terms generally reinforce the dominant QG forcing terms, whereas for anticyclones they have opposing signs and reduce the net right-side forcing.

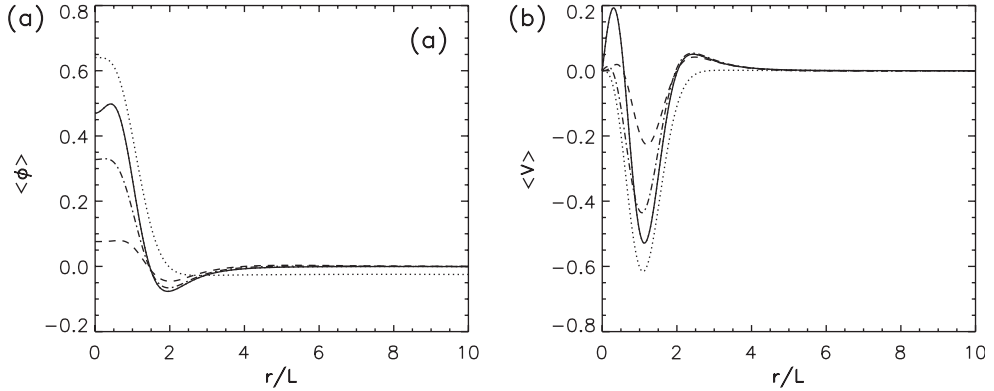


Figure 5. (a) $\langle \hat{\phi} \rangle_M(r)$ normalized by VfL and (b) $\langle \bar{v} \rangle_M(r)$ normalized by V for the standard cases defined in section 3: CYCLONE = solid line; ANTICYCLONE (with the sign reversed) = long-dash line; QG = dash-dot line; BT = dot line. The radius is normalized by L .

The BT changes in figure 5 are larger than the QG changes (with finite L_d) for the same reason as the difference in ϕ' amplitudes, viz., the elliptic operator inversion in (29) gives a larger response for similar right-side forcing without the second term associated with vortex stretching. The resulting difference is larger for the vortex changes than the fluctuations since the ϕ/q ratio is larger for the vortex-change response because the left-side operator lacks the terms associated with the azimuthal second derivatives in (24).

We use several norms to assess the vortex evolution under strain (section 2). The fluctuation and bracket norms from (15) are positive quadratic functionals of ϕ' and $\langle \phi \rangle$, respectively. Consequently, these norms exhibit a combination of both transient spiking and monotonic growth during the strain-impulse period, reflecting the pattern of perturbation growth. To assess the overall vortex change, however, we use the full SWE energy and potential enstrophy norms. The SWE energy change for the azimuthal-averaged vortex (16) is evaluated for these solutions. We focus on the irreversible change that occurs for $t \geq t_{max}$, and we make the approximation $m \ll 1$. The result is

$$\Delta \bar{E}_{swe} \approx 2\pi \int_0^\infty dr r \left(\bar{h} \bar{v} \langle v \rangle + \frac{1}{g} (\bar{\phi} + \frac{1}{2} \bar{v}^2) \langle \phi \rangle \right) \quad (35)$$

evaluated at $t = t_{max}$. The magnitude of $\Delta \bar{E}_{swe}$ is $\mathcal{O}(m^2 HL^2 V^2)$. The third term in the integrand is smaller than the first two terms by $\mathcal{O}(Ro)$. Thus, the essential cause for vortex weakening by external strain, as measured by this energy norm, is contained within the first radial boundary-value problem in (29) and its associated velocity relations (31) that yield radially integrated negative correlations between the mean vortex and its strain-induced change for both the mass field ($\bar{\phi} \langle \phi \rangle < 0$ on average) and the azimuthal velocity ($\bar{v} \langle v \rangle < 0$). The values of $\Delta \bar{E}_{swe}$ for the standard cases in section 3 are listed in table 1. In all the cases, strain weakens the mean vortex energy, and it does so much more for a cyclone than an anticyclone.

The analogous measure for the energy change associated with the azimuthal fluctuations is defined in (17). Again making the approximation $m \ll 1$ and noting

Table 1. Strain-impulse norms.

CASE	$\Delta \bar{E}'_{swe}$	$\Delta E'_{swe}$	$\Delta \bar{V}'_{swe}$	$\Delta V'_{swe}$
CYCLONE	-3.50	1.83	-54.2	16.7
ANTICYCLONE	-1.04	0.35	-1.74	0.48
QG	-3.02	1.21	-8.84	2.32
BT	-4.41	1.50	-5.03	2.10

The energy and potential enstrophy norms evaluated from (35)–(47) at $t = t_{max}$ and normalized by $m^2 HL^2 V^2$ for energy and $m^2 V^2 / g^2 H$ for enstrophy.

that all odd powers of the azimuthal fluctuations in E_{swe} have zero azimuthal average, the appropriate norm is

$$\Delta E'_{swe} \approx \int_0^{2\pi} d\lambda \int_0^\infty dr r \left(\frac{1}{2} \left(\bar{h}(u^2 + v^2) + \frac{1}{g} \phi'^2 \right) + \frac{1}{g} \bar{v} \phi' v' \right) \quad (36)$$

evaluated at $t = t_{max}$. The magnitude of $\Delta E'_{swe}$ is $\mathcal{O}(m^2 HL^2 V^2)$, i.e., the same as $\Delta \bar{E}'_{swe}$. The final term in the integrand is smaller than the first three terms by $\mathcal{O}(Ro)$. Since the dominant first three terms are positive-definite in $\Delta E'_{swe}$, a strain-impulse acts primarily to increase the energy associated with azimuthal fluctuations. The values of $\Delta E'_{swe}$ for the standard cases in section 3 (table 1) are all positive, indicating the generation of fluctuations by straining. The fluctuation energy change is much greater for cyclones than for anticyclones.

The SWE potential enstrophy change norms (15) at $t = t_{max}$, with the same approximations as for the energy norms, are the following:

$$\begin{aligned} \Delta \bar{V}'_{swe} &\approx 2\pi \int_0^\infty dr \frac{r \bar{q}}{2g} (2\langle \zeta \rangle - \bar{q}(\phi)) \\ &\rightarrow 2\pi \frac{f^2}{g^2 H} \int_0^\infty dr r \left(\frac{\bar{\zeta}}{f} - \frac{\bar{\phi}}{gH} \right) \left(\frac{\langle \zeta \rangle}{f} - \frac{\langle \phi \rangle}{gH} \right) \\ \Delta V'_{swe} &\approx \int_0^{2\pi} d\lambda \int_0^\infty dr \frac{r}{2g^2 \bar{h}} (\zeta'^2 + \bar{q}^2 \phi'^2 - 2\bar{q} \zeta' \phi'). \end{aligned} \quad (37)$$

The magnitude for both these norms is $\mathcal{O}(m^2 V^2 / g^2 H)$. The arrow in (37) indicates the leading-order expression in the QG limit for the enstrophy vortex change norm; its magnitude is formally smaller than the magnitude of the first expression by a factor of Ro , since evaluating the first expression with $\bar{q} = f/H$ gives a trivial result with $\langle \phi \rangle$ and $\langle \zeta \rangle$ obtained from (32)–(34).

The vortex change and asymmetric fluctuation enstrophy norms in table 1 indicate the same relative differences between cyclones and anticyclones. The enstrophy differences are even larger than for energy, mainly because the \bar{h}^{-1} weights in (37) greatly accentuate them. The BT energy changes are larger than the QG ones, and the enstrophy changes are somewhat smaller. These outcomes are based on the competing effects of larger barotropic amplitude (figures 4 and 5) — favoring larger BT changes — and the absence of the effects of changes in depth (i.e., terms involving ϕ) in the barotropic form of (35)–(37), whose signs in QG act to reinforce the remaining terms — favoring larger QG changes.

In summary, an external strain flow acts to weaken a vortex, and this is most cleanly demonstrated with the strain-impulse approximation used in this section.

External strain induces larger vortex changes for cyclones than anticyclones and larger changes for barotropic vortices than quasigeostrophic ones. The mean energy and enstrophy change norms in table 1 summarize the net vortex weakening.

6. Vortex recovery by VRWs

This section describes how a vortex recovers from a strain-induced perturbation, and it quantifies the net effect of a straining event on the vortex. The straining period specified in section 3 has a small duration t_{max} compared to the characteristic advective time scale L/V for the vortex relaxation process. The imposed strain flow induces an azimuthal wavenumber-two fluctuation at $t = t_{max}$ whose pattern is separable in r and λ as in (25). It has the same sign for all r values except for the radial sign change for ANTICYCLONE that occurs outside the vortex core (at $r \approx 2.5$ in figure 4). Thus, we can say that the initial value of a ‘local’ radial wavenumber on scales smaller than the vortex size is zero, i.e., $k(0) = 0$. This pattern can be seen in the upper left panel of figure 6 for q^{ab} defined in (7). During the relaxation phase, $t_{max} < t < \infty$, the mean angular velocity profile $\overline{\Omega}(r)$ causes the familiar differential rotation around the vortex whereby the spiral arms wrap up, propagate outward, and ultimately filament (Montgomery and Kallenbach 1997, MGM03); this is shown for CYCLONE in the subsequent panels of figure 6. This behavior is represented by a $k(t)$ that grows monotonically in time in association with an increasing number of sign changes in q^{ab} along all radial lines, and it is also associated with systematically decaying fluctuation geopotential and velocity amplitudes.

Figure 7 shows $|q^{ab}|(r, t)$ for CYCLONE and ANTICYCLONE. The patterns indicate an outward radial propagation of the asymmetric fluctuations in both cases. The stagnation radius (i.e., the limit of outward propagation) for the primary wave in CYCLONE is at approximately $1.8L$. This is noticeably larger than the stagnation radius for the ANTICYCLONE, which is $1.3L$, and also larger than in QG and BT, which both have a stagnation radius of $1.5L$. The stagnation radius is controlled by the radial group velocity of the VRWs. Within the context of waves in slowly varying media (i.e., a WKB approximation), the radial group velocity (equation (62) of MGM03) is controlled by the mean-vortex potential vorticity gradient $\overline{G}(r)$ and the radial wavenumber k . In CYCLONE, \overline{G} is negative everywhere since $\overline{q}(r)$ is monotonically decreasing (figure 3b), and k becomes positive. Since the radial group velocity is negatively correlated with the product of \overline{G} and k , this yields a positive value, and thus an outwardly directed propagation. In ANTICYCLONE, \overline{G} and k both have opposite signs compared to CYCLONE, but their product is the same, so this case also exhibits an outward group velocity.

From (4) and (7), \overline{G} can be expanded into

$$\overline{G} = \frac{\overline{\xi}}{\overline{\eta}} \left(\partial_r \overline{\xi} - \frac{\overline{q}}{g} \partial_r \overline{\phi} \right). \quad (38)$$

When terms of $\mathcal{O}(\text{Ro})$ are quantitatively important, $(\overline{\xi}, \overline{\eta})$ are larger for cyclones because their component terms are additive, whereas they are smaller for anticyclones because the terms have opposite signs and thus partially cancel. In contrast \overline{h} is smaller for cyclones for an analogous reason, and this change is dominant compared to $\overline{\eta}$ in

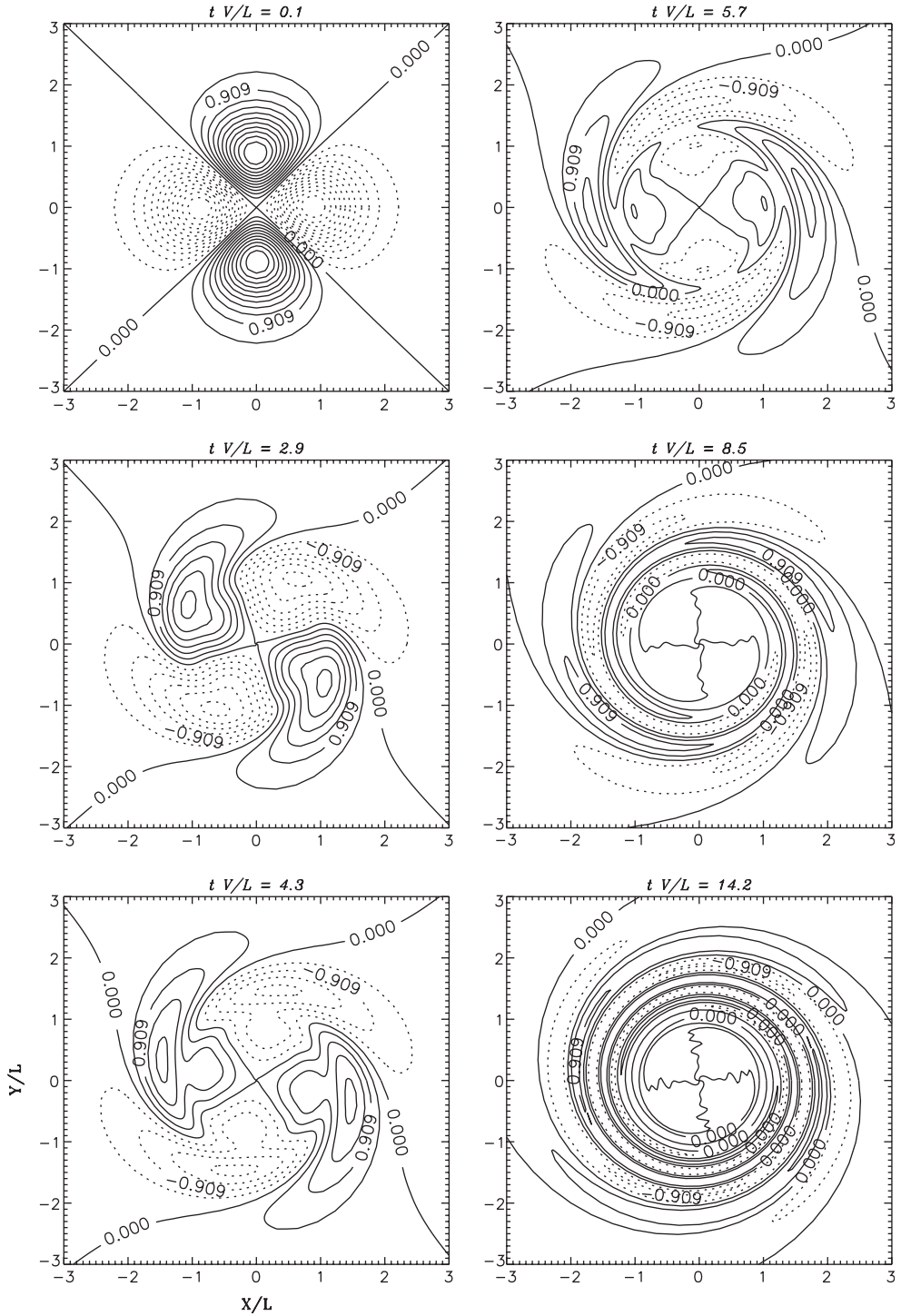


Figure 6. Swirl plots for $q^{ab}(x,y)$ normalized by mfV/L in CYCLONE at several times tV/L during the relaxation phase after impulsive strain.

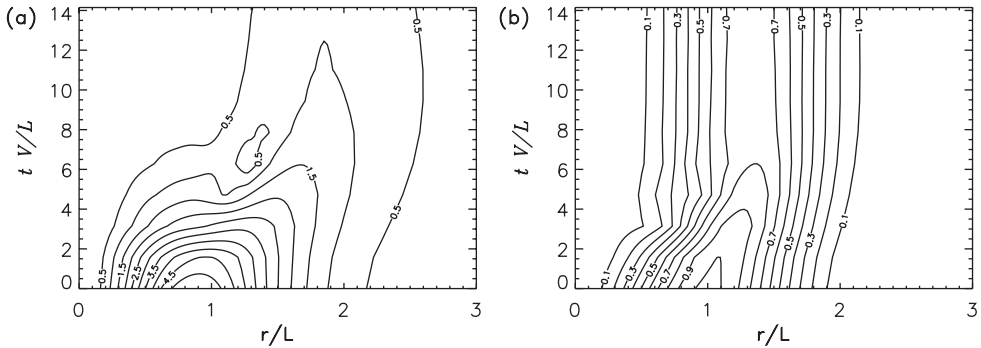


Figure 7. Hovmüller plots of $\max_{\lambda}[|q^{ab}|](r, t)$ normalized by mfV/L after impulsive strain in (a) CYCLONE and (b) ANTICYCLONE. The contour interval is 0.5 in (a) and 0.1 in (b).

making \bar{q} larger: $\partial_r \bar{\phi}$ is larger for cyclones because of gradient-wind balance (2), and for both vortex parities it combines additively with $\partial_r \bar{\zeta}$ with a further weighting by \bar{q} in (38). As a result of these differences, the magnitude of \bar{G} is significantly larger for cyclones than anticyclones, so are the group velocity and the stagnation radius (figure 3b). The outward radial group velocity causes a rapid evacuation of fluctuation potential vorticity in the core of the vortex that occurs in conjunction with the spiral wind-up of the primary wave packet. The core evacuation is also due to the outwardly directed group velocity, and it begins fairly early. The outward propagation of asymmetric potential vorticity is evident in the spiral plots of $q^{ab}(r, \lambda)$ in the core of both cyclones (figure 6) and anticyclones.

Because of the conservation of wave action and wave activity for VRWs (MGM03), amplitude decay of the primary wave packet is expected for an outwardly propagating VRW. Comparing the net change in q^{ab} during the relaxation phase, there is clearly a greater amount of fluctuation decay in CYCLONE than in ANTICYCLONE. The magnitude of the strain-induced fluctuation $|\phi'_i|(t_{max})$ in CYCLONE is larger than in ANTICYCLONE, with the QG and BT cases lying in between (figure 4). The $|q^{ab}|(t_{max})$ differences among the cases are even larger, with a ratio of about a factor of 5 between CYCLONE and ANTICYCLONE. In the absence of any dissipation for the fluctuations, the combination of greater cyclonic q^{ab} after straining and its greater relative decay during the relaxation phase suggests there must be a much greater strengthening of the cyclonic vortex through eddy–mean interaction in (13). Since the fluctuation is originally created by transfer from the mean vortex (i.e., strain weakening), this VRW relaxation strengthening is an opposite effect. As evident in figure 2, however, the strengthening is less than the weakening in all cases.

Figure 8 shows the temporal decay of the fluctuation geopotential amplitude for the four principal cases at the radius of maximum mean potential-vorticity gradient after the external strain is turned off. The evolution of the geopotential at the radius of maximum mean potential-vorticity gradient serves to identify whether the relaxation response is dominated by a single VRW quasi-mode (with exponential decay; Schecter *et al.* 2002) or a collection of sheared (continuum) VRWs that decay algebraically with time (MGM03). From figure 8 it is evident that the decay is only persistently exponential in BT. Decay in QG is less persistently exponential, if at all. CYCLONE and ANTICYCLONE exhibit highly non-exponential decay. These results suggest that the sheared VRW paradigm is the most appropriate one for the finite-Ro

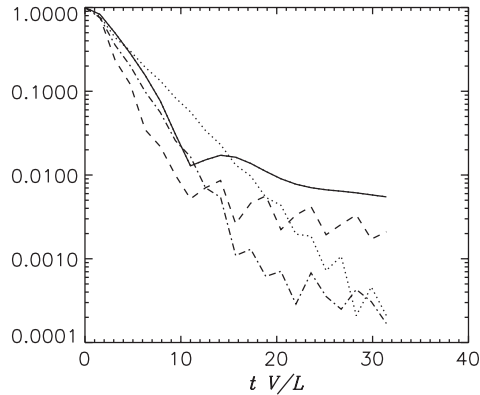


Figure 8. Decay of $|\phi'|$ at the radius of maximum mean potential vorticity gradient ($r \approx 0.6L$) during the vortex relaxation phase (starting at $t = t_{max}$), normalized by its value at t_{max} . CYCLONE = solid line; ANTICYCLONE = long-dash line; QG = dash-dot line; BT = dotted line.

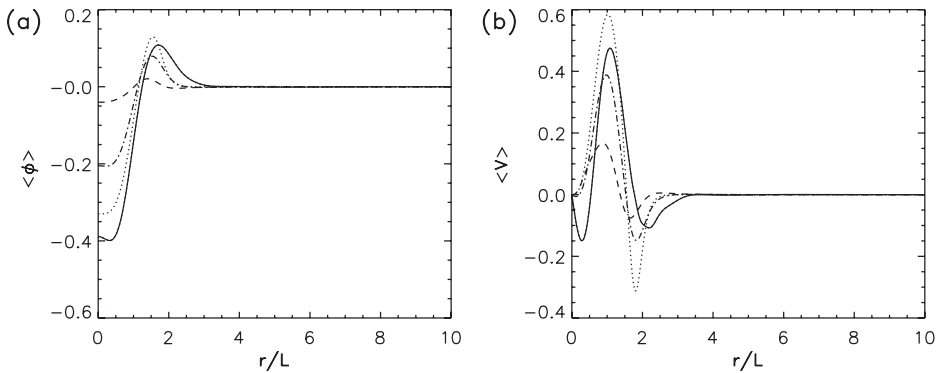


Figure 9. Vortex changes during the VRW relaxation phase following impulsive straining (i.e., between $t = 31.4$ and $t = t_{max}$): (a) $\langle\phi\rangle(r)$ normalized by $m^2 V/L$ and (b) $\langle v\rangle(r)$ normalized by $m^2 V$. CYCLONE = solid line; ANTICYCLONE (with the sign reversed) = long-dash line; QG = dash-dot line; BT = dotted line.

cyclonic/anticyclonic vortex recovery phase. In general, we expect that the relaxation response will involve a superposition of VRWs and/or quasi-modes, but we have not made any attempt to decompose the fluctuation field into individual ‘pure tones’.

Figure 9 shows the net geopotential vortex change $\langle\phi\rangle$ at $t = 31.4L/V$ minus its value at the end of the straining period, $t = t_{max}$. A bimodal structure in $\langle\phi\rangle$ is clearly evident for all four cases, with a large negative value inside the radius of maximum wind for $\bar{v}(r)$ and a smaller positive value outside. The negative $\langle\phi\rangle$ corresponds to a greater mean central depression in h for a cyclone and, by gradient-wind balance, a stronger vortex. Since the cyclonic $\langle\phi\rangle$ exhibits a peak amplitude that is approximately twice that of the anticyclonic case (plotted here with a sign reversal), this implies that the cyclone undergoes a greater recovery from the strain weakening. Note that the peaks in $\langle\phi\rangle$ for the cyclone are slightly outside the others due to the larger radial propagation of the corresponding VRWs. Again, the QG and BT results typically lie in between CYCLONE and ANTICYCLONE.

From equation (33) of MGM03, relating the time derivative of balanced fluctuations to the wave-induced acceleration of the azimuthal velocity, the larger response in $\langle v\rangle$ in

the cyclone seen in figure 9 is traceable to the larger radial propagation in the cyclone in an approximate pseudo-momentum rule in the limit of small but finite Ro . For the BT case with non-divergent flow, the physical interpretation of this wave-induced acceleration is a familiar one. As the mean angular velocity causes the fluctuation to wrap around the vortex, the phase lines tilt in the direction of the shear. This generates an eddy angular momentum flux that is convergent on the inward side of the waves, and divergent on the outward side. Since the mean tangential velocity is negatively correlated with the divergence of the eddy momentum flux, this implies an increase in $\langle v \rangle$ on the inward side of the waves and a decrease on the outward side. This feature is seen in figure 9 for all the four cases, and implies a vortex strengthening in the core. Note that the positive inner peak is larger than the negative one outside the core. Since the total angular momentum of the fluid must be conserved during the relaxation phase, the VRWs only redistribute angular momentum, $r\langle v \rangle$. Thus at the smaller inner radius, the vortex change must be larger in magnitude to balance the opposite-sign change at the larger outer radius. Since the majority of the wave-mean flow interaction occurs near the stagnation radius, the zero value in $\langle v \rangle$ will occur near this location. The profile of $\langle v \rangle$ for CYCLONE, with its larger VRW stagnation radius, is thus shifted outwards compared to the other cases.

The energy and potential enstrophy vortex change norms (15)–(16) quantify the area-integrated vortex change (figure 2). These measures are approximately controlled by $\langle \phi \rangle$ and $\langle v \rangle$ as indicated in (35) and (37). After the initial (and here brief) strain-weakening in these norms, both energy and enstrophy plots increase rather sharply at early times as the recovery begins, but asymptote after a time of about $t = 8L/V$, corresponding to a little more than one eddy turn-around time. After this point, the fluctuations have become significantly wrapped around the vortex so that their phase lines are almost aligned with the mean swirl flow, so the eddy momentum fluxes become small. The recovery phase for CYCLONE can be seen to be larger in magnitude for both energy and enstrophy compared to ANTICYCLONE, as can be anticipated by the larger peaks in $\langle \phi \rangle$ and $\langle v \rangle$ during this time. Since the strain-induced weakening is so much larger for CYCLONE despite this greater strengthening, its late-time asymptotic values are still more negative than for ANTICYCLONE (with the QG case in between), which indicates a greater net weakening for CYCLONE.

The net vortex changes in $\langle \phi \rangle$ and $\langle v \rangle$ over both the straining period and relaxation phase are in figure 10. Note that $\langle \phi \rangle$ shows larger positive values for CYCLONE than ANTICYCLONE, and in fact for CYCLONE it is almost exclusively positive which demonstrates weakening of the vortex at almost all radii. In $\langle v \rangle(r)$, ANTICYCLONE has larger-magnitude peaks than CYCLONE, which would suggest more anticyclonic weakening. However, the mean energy and enstrophy changes depend more heavily on the changes in $\langle \phi \rangle(r)$ where the cyclone is more heavily weakened. The large peaks in both $\langle \phi \rangle$ and $\langle v \rangle$ for the BT case reflect the difference in the ϕ/q strain–response ratio due to the absence of vortex-stretching term when $\bar{\gamma} = 0$ (section 5). The manifestation of the larger vortex change profiles in the energy and enstrophy change norms (i.e., larger $\Delta \bar{E}_{swe}$, smaller $\Delta \bar{V}_{swe}$; figure 2) reflects a subtle competition between the velocity and geopotential components in (35) and (37).

In summary, during the relaxation phase, the perturbed vortex exhibits the following behaviors. For a fluctuation in the absence of further external straining, there is radial propagation; azimuthal wrap-up and (r, λ) phase-line tilting down the gradient of $\bar{\Omega}(r)$; and rapid amplitude decay in fluctuation geopotential and velocity. The effect of the

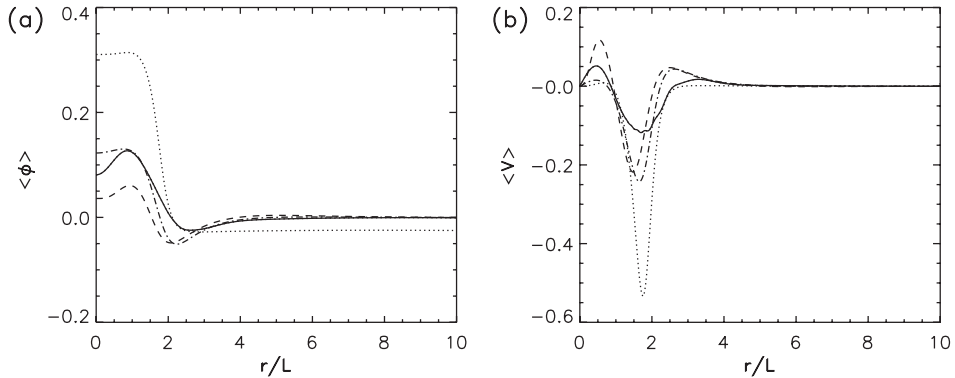


Figure 10. Net vortex change in (a) $\langle\phi\rangle(r)$ normalized by $m^2 V f L$ and (b) $\langle v\rangle(r)$ normalized by $m^2 V$ over the full time integration, including both the impulsive straining and relaxation phases. CYCLONE = solid line; ANTICYCLONE (with the sign reversed) = long-dash line; QG = dash-dot line; BT = dot line.

mean eddy fluxes on the vortex is to strengthen it in both energy and enstrophy during this period of strong phase-line rotation. Based on an extensive survey of vortex-relaxation solutions (not reported here), we have found no pervasive differences between the relative efficiency of cyclonic and anticyclonic strengthening due to this process. This is consistent with the similar proportional changes seen here in CYCLONE and ANTICYCLONE. Thus, we conclude that the essential cause of anticyclonic dominance is the smaller strain weakening for anticyclones (section 5). All of these fluctuation and vortex-change behaviors are consistent with previous studies of VRWs and quasi-modes (e.g., MGM03; Schecter *et al.* 2000).

7. Sensitivities

7.1. Deformation radius

For the primary cases presented in section 3, $Ro = 0.2$, and $L_d/L = 1.11$. Here we examine cases with a Ro that is half as large, $Ro = 0.1$, to allow for smaller L_d values that would otherwise bottom-out; i.e., the cyclonic \bar{h} would vanish in the vortex core. Specifically, we compare cyclonic and anticyclonic solutions for three L_d/L values equal to 0.78, 1.11, and 1.57 (corresponding to mean depths of $H = 25$, 50, and 100 m). When L_d/L is large enough, the flow becomes essentially barotropic, a regime which has dynamical symmetry between cyclones and anticyclones. We would expect then that as we move further from the barotropic regime (i.e., decreasing L_d/L), we should begin to see a clear distinction between cyclones and anticyclones.

Figure 11 shows $\langle v\rangle(r)$, for the three L_d/L values. As L_d/L decreases, not only do both cyclones and anticyclones have a reduced peak value, but the cyclonic and anticyclonic profiles diverge as expected. This result is reflected in the mean enstrophy norm (i.e., (15)–(16) and (37)) and summarized in table 2 for the ratio of the late-time ($t = 31.4L/V$) enstrophy change norms, $\Delta\bar{V}_{swe}$, for cyclonic and anticyclonic mean vortices. Since all cases demonstrate net vortex weakening, their mean norms are negative (with larger negative values for larger weakening). Thus ratios greater than one indicate anticyclonic dominance, which increases as the ratio grows. We have

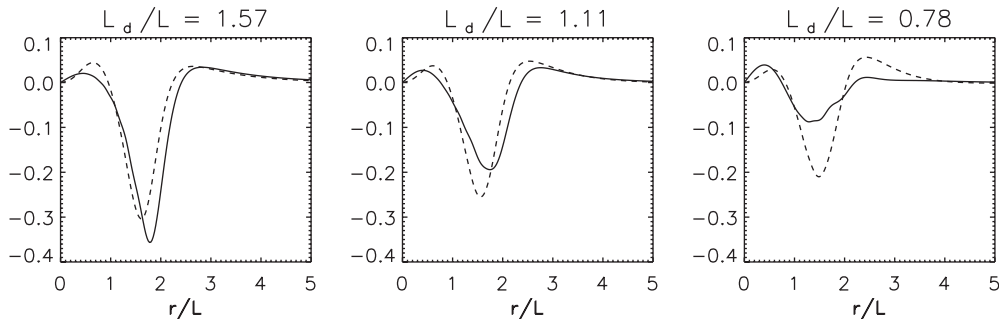


Figure 11. Changes in $\langle v \rangle(r)$ normalized by $m^2 V$ at $t = 31.4L/V$ for CYCLONE (solid line) and ANTICYCLONE (long-dash line, with the sign reversed) with impulsive strain forcing and different values of L_d/L .

Table 2. Cyclone/anticyclone norm ratios.

Ro	L_d/L	$\Delta \bar{V}_{swe}$ ratio
0.1	1.57	1.86
0.1	1.11	3.29
0.1	0.78	10.3
0.2	1.11	20.9

The ratio of late-time (i.e., $t = 31.4V/L$) cyclonic and anticyclonic vortex change enstrophy norms with impulsive strain and different values of L_d/L .

also included the value for the primary cases given in sections 4 and 5 for comparison (where $Ro = 0.2$).

In the norms the term involving $\langle v \rangle$ has the most sensitivity to changes in L_d , although the vortex change geopotential, $\langle \phi \rangle$, also has an important contribution. The energy norm is not so monotonic in its sensitivity to changes in L_d/L , so it is thus a less useful integral measure to compare cyclonic and anticyclonic dependences on L_d/L .

7.2. Rossby number

Our investigation is limited in Ro by the disappearance of cyclone–anticyclone differences as $Ro \rightarrow 0$ (i.e., QG) and the vanishing of $\bar{h}(r=0)$ as Ro increases in cyclones for a given value of L_d/L . In the SWE with the mean vortex profile (18) and $L_d/L \approx 1$, this upper bound on Ro comes into force before the centrifugal instability boundary (i.e., $\bar{\zeta}(r=0) = -f$) for anticyclones. Within this Ro range we have found no surprises. Typically CYCLONE and ANTICYCLONE results diverge from QG in opposite ways as Ro increases (e.g., figure 4 *et seq.*), and their differences vanish smoothly as Ro decreases (e.g., table 2).

7.3. Strain duration

Sections 3–5 focus on cases with only a brief duration of the external strain flow, $t_{max} \ll L/V$. As also done in BG99, we have examined various solutions with

$t_{max} \sim L/V$ and found no qualitative changes in the phenomena but an increased complexity, because the strain-induced fluctuations are continuously generated while the VRW wrap-up is in progress; furthermore, the vortex change norms become more oscillatory in time. However, there are interesting differences when the external strain is sustained in time, $t_{max} \gg L/V$, and this regime is examined in section 8.

7.4. Wave nonlinearity

The model we are using is a quasi-linear one: the fluctuation dynamics are linear, but the mean vortex changes are due to averages of nonlinear fluctuation products. We wish to address the extent to which this linear wave approximation is appropriate for the primary cases presented in this article, and also to establish the amplitude of the external strain flow at which the nonlinear effects become important. To this end we add in the nonlinear wave–wave interactions, in particular the interactions between wavenumber-two fluctuations to produce wavenumber-four fluctuations, which in turn interacts with itself to contribute to the vortex change and with the wavenumber-two fluctuation back onto the wavenumber-two fluctuation.

We examine the QG case as the simplest and the most straightforward one. In the primary QG case (section 3) but with added wave–wave terms, there are essentially no important differences due to wave–wave nonlinearity. The amplitude of the induced wavenumber-four fluctuation is about four orders of magnitude smaller than the primary wavenumber-two fluctuation, so this result is not surprising. Consistent with this result as a guideline, it is not until the external strain flow has an amplitude α that is about 2000 times larger than that used in the primary case (section 3) that the wavenumber-four and -two amplitudes become comparable, and thus the wave–wave effects become more significant. Note that with this $\alpha = 2 \times 10^{-4} \text{ s}^{-1}$, the external strain velocity (19) at $r=L$ is 10 times larger than the mean vortex V . (Alternatively, with a larger strain duration t_{max} a smaller α could achieve the same effect.) This shows that the wave nonlinearity is significant only in extreme cases.

Since the wavenumber-four pattern has twice as many oscillations azimuthally around the vortex, the combined fluctuation pattern strengthens in some places and weakens in others compared to the wavenumber-two pattern alone. Also, the wavenumber-four peak is located further out radially than the wavenumber-two peak, so the combined pattern is a modulated wavenumber-two pattern. It does, however, windup spirally as before, with the underlying behavior being similar. Further, the mean norms display only small differences from the primary QG case, with approximately a 6% change in end-state behavior for the mean energy, and about 2% change for mean enstrophy, where both changes reflect less net weakening of the vortex. Thus even at much larger external strain flow amplitudes, the wave–wave effects, while noticeable, still do not significantly alter the qualitative behavior of the vortex. Our choice to use linearized waves at the amplitudes chosen for the primary cases is therefore a reasonable one.

For vortices that are linearly stable (as the one investigated here) and exhibit a generally decaying fluctuation amplitude, we can expect another nonlinear effect even when α is not very large. For a uniform plane-shear flow, the wrapped-up filaments of fluctuation potential vorticity are susceptible at long times to secondary barotropic instabilities associated with their ever-increasing local gradient (Haynes 1987, Vanneste 1999). It is likely that this phenomenon occurs in vortices as well.

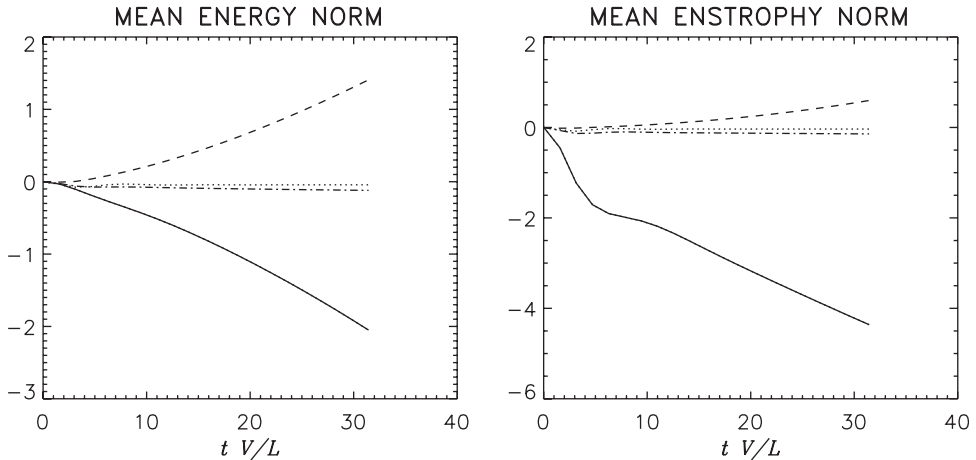


Figure 12. History of the vortex change norms for (left) energy, $\Delta \bar{E}_{\text{swe}}(t)$, and (right) potential enstrophy, $\Delta \bar{V}_{\text{swe}}(t)$, for the primary cases with sustained external strain: CYCLONE = solid line; ANTICYCLONE = long-dash line; QG = dash-dot line; and BT = dotted line. Normalizations are in table 1.

However, its consequences should be limited to the late-stage evolution of the fluctuations after the period in which their eddy–mean interaction is largely over, so we do not investigate that process here.

8. Sustained strain

Section 4 described how vortices react to an impulsive strain. Here we impose the same external strain, but after the ramp-up period ($t > t_{\text{max}}/2$), the amplitude is fixed throughout the runs (i.e., $F(t) = 1$). Thus we will see a combination of both the strain response (section 4) and the relaxation from that response (section 5). We made runs for all four primary cases: CYCLONE, ANTICYCLONE, QG, and BT.

Figure 12 shows the mean vortex energy and enstrophy change for all the four cases. Note the dramatic difference between CYCLONE and ANTICYCLONE: the cyclone exhibits a continual strong vortex weakening, while the anticyclone, after an initial weakening response (section 4), begins to strengthen and continues to do so. The QG and BT vortices undergo net weakening, with relatively small amplitudes compared to the cyclone. Their weakening, however, occurs in an oscillatory fashion that is not clearly visible here due to their small amplitude. In particular, the QG vortex has an initial weakening, followed by a partial recovery, and then a continued weakening. The BT vortex initially weakens, but then oscillates until it asymptotes to a constant negative value for both mean energy and enstrophy. This last case is qualitatively very similar to the results reported in BG99 (their figure 4).

As the external strain turns on, all the four cases initially have a response as discussed in section 4. The strain induces a wavenumber-two fluctuation by elongating the mean vortex into an elliptical shape. These fluctuations then attempt to relax as VRWs (section 5), yet must do so while still immersed in the external strain flow. The VRWs begin to wind up spirally, but are impeded by the fixed strain flow. This prevents axisymmetrization of the vortex, so the vortex remains elliptical, reaching

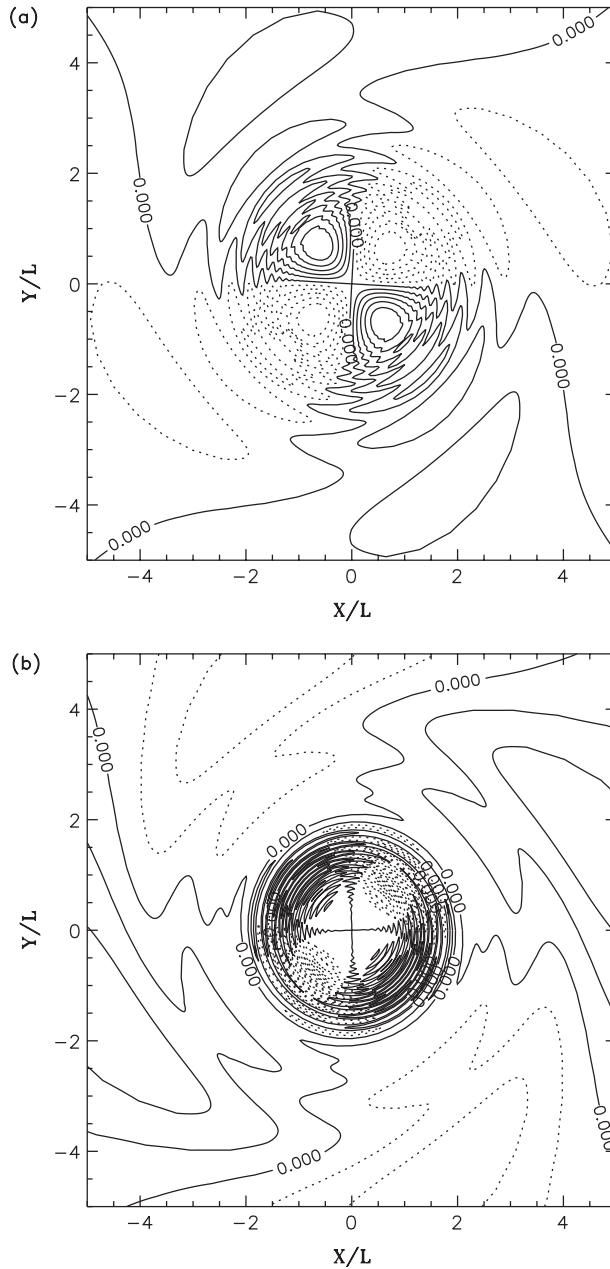


Figure 13. Swirl plots for $q^{ab}(x, y)$ normalized by fV/L at $t = 31.4L/V$ in (a) CYCLONE (with contour interval 0.117) and (b) ANTICYCLONE (with contour interval 0.025 and the sign reversed) under sustained external strain. Negative contours are dashed, and the zero contours are labeled.

equilibrium with a standing-wave fluctuation pattern oriented 45° counter-clockwise from the initial strain induced location. This can be seen in the late time swirl plots of normalized q^{ab} for both the cyclone and anticyclone in figure 13. Compare this with figure 6 which demonstrates axisymmetrization. This 45° orientation of the

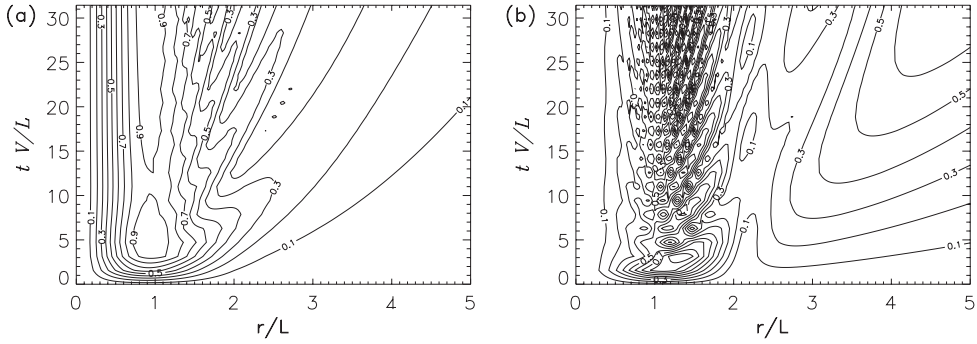


Figure 14. Hovmüller plots of $\max_{\lambda}[q^{ab}](r, t)$ under sustained external strain. The fields are normalized by their maximum value near $r=L$ and $t=3L/V$: (a) CYCLONE (max value = $0.736 fV/L$) and (b) ANTICYCLONE (max value = $0.095 fV/L$). The contour interval is 0.1.

vortex under sustained strain was also demonstrated by BG99 for the BT case (their figure 7a). This is in stark contrast to the behavior of an initially circular vortex patch placed into a weak, steady straining flow, which oscillates continually between circular and elliptical states (Kida 1981; BG99). The reason for this behavior is explained by BG99: a vortex patch does not exhibit the spiral wrap-up of q contours, thus arresting the irreversible transfer of enstrophy to small scales, and making it impossible for the vortex to relax to the stable, steady-state solution of an elliptical vortex patch with its major axis tilted 45° relative to the strain axes (Moore and Saffman 1971).

As the vortex fluctuations evolve into the configuration in figure 13, they interact with the external strain resulting in mean vortex weakening for the cyclone and strengthening for the anticyclone. This can be seen by identifying the dominant terms in the vortex change azimuthal velocity equations (8) and (10) as

$$\partial_t \langle v_i \rangle \approx -\langle \Sigma N^v \rangle \approx -\langle u'_e \zeta'_i \rangle, \quad (39)$$

where the fluctuation relative vorticity is

$$\zeta'_i = \frac{1}{r} \partial_r (r v'_i) - \frac{1}{r} \partial_\lambda u'_i. \quad (40)$$

However, the fluctuations are not lost through this interaction because they are continually reinforced by interaction between the mean vortex and the external strain (even growing in the outer region of the anticyclone; figure 14). Thus individual parcels rotate around the vortex, but the waves are relatively locked in a standing eddy pattern. There is some exception to this, as seen by the increasing development of fine structure in the inner core region, where there is competition between the fixed external strain and the VRW tendencies for spiral wrap-up and radial propagation.

These swirl plots highlight other interesting and telltale features of the vortex evolution under sustained strain. Both the cyclone and, to a larger degree, the anticyclone develop a distinct outer region, which for the anticyclone both grows and has the opposite sign to the inner core region. The vortex strengthening of the

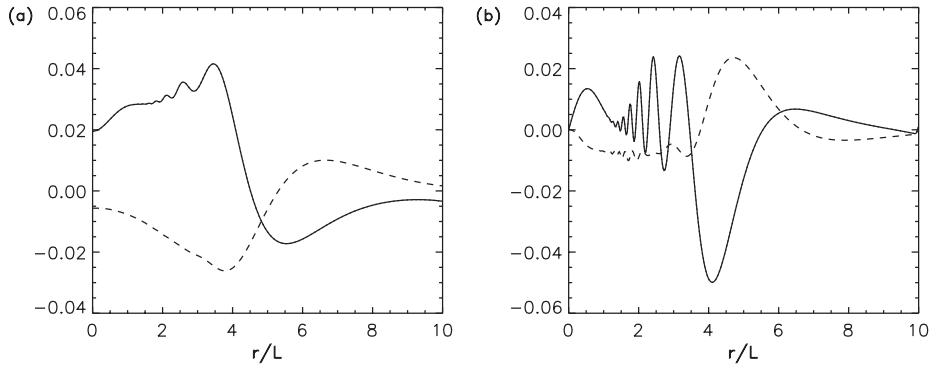


Figure 15. Changes in (a) $\langle \phi \rangle(r)$ (normalized by $m^2 V f L$) and (b) $\langle v \rangle(r)$ (normalized by $m^2 V$) at $t = 31.4L/V$ for CYCLONE (solid lines) and ANTICYCLONE (long-dash lines, with the sign reversed) under sustained external strain.

anticyclone (as compared with the weakening for the cyclone) is essentially due to this difference. Looking back at the impulsive strain-induced fluctuation geopotential for the different cases in section 4 (figure 4), the anticyclonic vortex response in the outer core has a fluctuation of opposite sign to the inner core, while the other cases do not. Although the $\mathcal{O}(1)$ forcing term in (24) switches sign between cyclones and anticyclones, the $\mathcal{O}(Ro)$ terms (i.e., the second right-side group within the square brackets proportional to $\bar{\gamma}^2$) do not. Thus the forcing terms are additive in cyclones and partially canceling in anticyclones, such that at large radius the sum of the anticyclonic forcing terms is opposite in sign to the core. It is this outer anomaly that grows and propagates outwards radially which acts to strengthen the vortex. This can be seen in the Hovmüller plots of normalized $|q^{ab}|(r, t)$ in figure 14. These demonstrate not only the radial propagation of the VRWs, but also their growth, as well as the development of inner core fine structure. Note that the outer fluctuations do not stagnate, and that the anticyclonic fluctuation continues to grow fairly rapidly as long as the external strain is sustained.

These fluctuations interact primarily with the external strain to produce a mean vortex change response in geopotential $\langle \phi \rangle$ and azimuthal velocity $\langle v \rangle$. The end-time values are plotted in figure 15. Note the correspondence between the outer-region location of the fluctuations and the signal in $\langle v \rangle$ that in the norms contributes to weakening for cyclones and strengthening for anticyclones. The plots of $\langle \phi \rangle$ show the controlling element responsible for vortex weakening in the cyclone and strengthening for anticyclone in the core region.

The key difference between the cyclone and anticyclone in the finite- Ro regime is the existence of an oppositely signed potential vorticity fluctuation in the outer core region of the anticyclone. This allows for a continual strengthening of the mean vortex as the strain-induced fluctuations interact with the fixed external strain. This continual strengthening can be seen even with Ro as small as 0.0375 when $L_d/L \approx 1$, so this sustained-strain growth is not just a large- Ro phenomenon. In the cyclone (and QG and BT vortices), the outer and inner fluctuations are of the same sign. This results in the familiar vortex weakening, demonstrated earlier in this article, that continues as long as the external strain is maintained.

From a meteorological perspective, this anticyclonic strengthening mechanism is partly distinct from previous explanations of persistent blocking anticyclones in the

mid-latitude troposphere. In addition to viewing the blocking flow configuration as a stable, nonlinear, stationary state (Charney and DeVore 1979, McWilliams 1980, Butchart *et al.* 1987), it has been argued that the anticyclonic vortex is further strengthened by up-scale eddy vorticity fluxes from remotely generated smaller eddies that impinge on the parent vortex (Green 1977, Shutts 1983). The demonstration here that fluctuations locally induced by sustained strain can strengthen an anticyclone with finite Ro suggests an alternative explanation for how atmospheric blocking is sustained.

9. Summary and prospects

Isolated coherent vortices in the interior regions of rotating, stratified flows undergo cycles of disruption by other flows in their neighborhood and recovery by axisymmetrization. In this study, we have idealized this cycle to the perturbation of an otherwise stationary vortex in the Shallow-water equations by a transient external strain flow followed by a relaxation phase in which linearized asymmetric fluctuations evolve as Vortex Rossby Waves (VRWs) by propagating in radius, wrapping around the mean vortex, decaying in energy, and forcing changes in the azimuthally averaged vortex. The tendency of these vortex changes is weakening during the straining phase and strengthening during the recovery phase, albeit typically only partially so that the outcome of the cycle is net weakening. Furthermore, for intermediate values of the vortex Rossby and Froude numbers, cyclones are more disruptable and have a greater net weakening than anticyclones for reasons that are understandable in terms of the response to an impulsive strain, independent of the subsequent VRW evolution. In the case of a sustained external strain flow, the same kind of disparity between cyclonic and anticyclonic responses occurs, except that a sufficiently strong anticyclone can manifest net strengthening.

We believe this is the likely explanation for the many reported examples of anticyclonic vortex dominance in the theoretical literature (section 1), as well as the apparently greater robustness of strong anticyclones in nature away from boundaries. Thus, we believe that strain-weakening, VRW-strengthening, and anticyclonic-dominance are generic behaviors for coherent, interior, rotating, stratified vortices, although it will be necessary to explore well beyond the idealizations in this study to adequately test this hypothesis.

Acknowledgments

LPG and JCM acknowledge support from the grant ONR N00014-95-1-0316. MTM acknowledges support from grants NSF-ATM-0132006, NSF-ATM-0101781, and ONR N00014-02-1-0474.

References

- Arai, M. and Yamagata, T., Asymmetric evolution of eddies in rotating shallow water. *Chaos*, 1994, **4**, 163–173.
- Bassom, A.P. and Gilbert, A.D., The spiral wind-up and dissipation of vorticity and a passive scalar in a strained planar vortex. *J. Fluid Mech.*, 1999, **398**, 245–270.

- Brickman, D. and Ruddick, B., The behavior and stability of a lens in a strain field. *J. Geophys. Res.*, 1990, **95**, 9657–9670.
- Briggs, R.J., Daugherty, J.D. and Levy, R.H., Role of Landau damping in crossed-field electron beams and inviscid shear flow. *Phys. Fluids*, 1970, **13**, 421–432.
- Butchart, N., K. Haines and Marshall, J.C., A theoretical and diagnostic study of solitary waves and atmospheric blocking. *J. Atmos. Sci.*, 1987, **46**, 2063–2078.
- Charney, J.G., Planetary fluid dynamics. In *Dynamic Meteorology*, edited by P. Morel, pp. 97–351, 1973 (Reidel Publishing Co.: Dordrecht, Holland).
- Charney, J.G. and Devore, J.G., Multiple flow equilibria in the atmosphere and blocking. *J. Atmos. Sci.*, 1979, **36**, 1205–1216.
- Cho, Y.Y.-K. and Polvani, L.M., The emergence of jets and vortices in freely evolving, shallow-water turbulence on a sphere. *Phys. Fluids*, 1996, **8**, 1531–1552.
- Cushman-Roisin, B. and Tang, B., Geostrophic turbulence and emergence of eddies beyond the radius of deformation. *J. Phys. Ocean.*, 1990, **20**, 97–113.
- Drijfhout, S.S., Why anticyclones can split. *J. Phys. Oceanogr.*, 2003, **33**, 1579–1591.
- Graves, L.P., Vortex evolution by straining and development of anticyclonic dominance. PhD dissertation, Dept. of Atmospheric and Oceanic Sciences, UCLA, 2005, p. 142.
- Green, J.S.A., The weather during July 1976: some dynamical considerations of the drought. *Q. J. Roy. Met. Soc.*, 1977, **96**, 157–185.
- Haynes, P.H., On the instability of sheared disturbances. *J. Fluid Mech.*, 1987, **175**, 463–478.
- Hoskins, B.J., The role of potential vorticity in symmetric stability and instability. *Q. J. Royal Met. Soc.*, 1974, **100**, 480–482.
- Kida, S., Motion of an elliptic vortex in a uniform shear field. *J. Phys. Soc. Japan*, 1981, **50**, 3517–3520.
- Lindzen, R.S. and Holton, J.R., A theory for the quasi-biennial oscillation. *J. Atmos. Sci.*, 1968, **25**, 1095–1107.
- Matsura, T. and Yamagata, T., On the evolution of nonlinear planetary eddies larger than the radius of deformation. *J. Phys. Ocean.*, 1982, **12**, 440–456.
- McWilliams, J.C., An application of equivalent modons to atmospheric blocking. *Dyn. Atmos. Oceans*, 1980, **5**, 43–66.
- McWilliams, J.C., Submesoscale, coherent vortices in the ocean. *Rev. Geophys.*, 1985, **23**, 165–182.
- McWilliams, J.C., Weiss, J.B. and Yavneh, I., Anisotropy and coherent structures in planetary turbulence. *Science*, 1994, **264**, 410–413.
- McWilliams, J.C., Diagnostic force balance and its limits. In *Nonlinear Processes in Geophysical Fluid Dynamics*, edited by O.U. Velasco Fuentes, J. Sheinbaum and J. Ochoa, pp. 287–304, 2003 (Kluwer Academic Publishers: Amsterdam).
- McWilliams, J.C., Graves, L.P. and Montgomery, M.T., A formal theory for vortex Rossby waves and vortex evolution. *Geophys. Astrophys. Fluid Dyn.*, 2003, **97**, 275–309.
- Melander, M.V., McWilliams, J.C. and Zabusky, N.J., Axisymmetrization and vorticity gradient intensification of an isolated two-dimensional vortex. *J. Fluid Mech.*, 1987, **178**, 137–159.
- Molemaker, M.J., McWilliams, J.C. and Yavneh, I., Ageostrophic baroclinic instability and loss of balance. *J. Phys. Ocean.*, 2004, **35**, 3720–3725.
- Moller, J.D. and Montgomery, M.T., Vortex Rossby waves and hurricane intensification in a barotropic model. *J. Atmos. Sci.*, 1999, **56**, 1674–1687.
- Montgomery, M.T. and Kallenbach, R.K., A theory for vortex Rossby waves and its application to spiral bands and intensity changes in hurricanes. *Quart. J. Roy. Meteor. Soc.*, 1997, **123**, 435–465.
- Moore, D. and Saffman, P., Structure of a line vortex in an imposed strain. *Aircraft Turbulence and its Detection*, pp. 339–354, 1971 (Plenum Press: NY).
- Nof, D., The role of angular momentum in the splitting of isolated eddies. *Tellus*, 1990, **42**, 469–481.
- Nof, D., Fission of single and multiple eddies. *J. Phys. Oceanogr.*, 1991, **21**, 40–52.
- Polvani, L.M., McWilliams, J.C., Spall, M.A. and Ford, R., The coherent structures of shallow-water turbulence: deformation-radius effects, cyclone/anti-cyclone asymmetry, and gravity-wave generation. *Chaos*, 1994, **4**, 177–186.
- Schecter, D.A., Dubin, D.H.E., Cass, A.C., Driscoll, C.F., Lansky, I.M. and O’Neil, T.M., Inviscid damping of asymmetries on a two-dimensional vortex. *Phys. Fluids*, 2000, **12**, 2397–2412.
- Schecter, D.A., Montgomery, M.T. and Reasor, P.D., A theory for the vertical alignment of a quasigeostrophic vortex. *J. Atmos. Sci.*, 2002, **59**, 150–168.
- Schecter, D.A. and Montgomery, M.T., On the symmetrization rate of an intense geophysical vortex. *Dyns. Atmos. Oceans*, 2003, **37**, 55–88.
- Shapiro, L.J. and Montgomery, M.T., A three-dimensional balance theory for rapidly rotating vortices. *J. Atmos. Sci.*, 1993, **50**, 3322–3335.
- Shutts, G.J., The propagation of eddies in diffluent jetstreams: eddy vorticity forcing of “blocking” flow fields. *Q. J. Roy. Met. Soc.*, 1983, **109**, 737–761.
- Stegner, A. and Dritschel, D.G., A numerical investigation of the stability of isolated shallow-water vortices. *J. Phys. Ocean.*, 2000, **30**, 2562–2573.

- Vanneste, J., A spatial analogue of transient growth in plane Couette flow. *J. Fluid Mech.*, 1999, **397**, 317–330.
- Yavneh, I. and McWilliams, J.C., Breakdown of the slow manifold in the shallow-water equations. *Geophys. & Astrophys. Fluid Dyn.*, 1994, **75**, 131–161.
- Yavneh, I., Shchepetkin, A.F., McWilliams, J.C. and Graves, L.P., Multigrid solution of rotating, stably stratified flows: the balance equations and their turbulent dynamics. *J. Comp. Phys.*, 1997, **136**, 245–262.